

Comparison of K^-p and K^+p Interactions,
and a Programmatic Study of Strange Quark Spectroscopy

D. Aston, W. Dunwoodie, S. Durkin, A. Honma, W. B. Johnson, P. Kunz,
D. W. G. S. Leith, L. Levinson, B. N. Ratcliff, R. Richter, S. Shapiro,
R. Stroynowski, S. Suzuki, G. Tarnopolsky, S. Williams.

SLAC, (Group B), Stanford University, California

N. Horikawa, S. Iwata, R. Kajikawa, T. Matsui, A. Miyamoto, T. Nakanishi,
Y. Ohashi, C. O. Pak, T. Tauchi.

Physics Dept., University of Nagoya, Nagoya

T. Shimomura and K. Ukai

Institute for Nuclear Studies, University of Tokyo, Tokyo

and

S. Sugimoto

National Lab. for High Energy Physics, KEK, Oho, Tsukuba, Ibaraki, Japan

SUMMARY

1. Title of Experiment: Comparison of K^-p and K^+p Interactions, and a Programmatic Study of Strange Quark Spectroscopy

2. Spokesmen: D. Aston, B. N. Ratcliff

Experimenters:

D. Aston, W. Dunwoodie, S. Durkin, A. Honma, W. B. Johnson, P. Kunz,
D. W. G. S. Leith, L. Levinson, B. N. Ratcliff, R. Richter,
S. Shapiro, R. Stroynowski, S. Suzuki, G. Tarnopolsky, S. Williams.

SLAC, (Group B), Stanford University, California

N. Horikawa, S. Iwata, R. Kajikawa, T. Matsui, A. Miyamoto,
T. Nakanishi, Y. Ohashi, C. O. Pak, T. Tauchi.

Physics Dept., University of Nagoya, Nagoya

T. Shimomura and K. Ukai

Institute for Nuclear Studies, University of Tokyo, Tokyo

and

S. Sugimoto

National Lab. for High Energy Physics, KEK, Oho, Tsukuba, Ibaraki, Japan

3. Summary

We propose to study K^+p and K^-p interactions at 11 GeV/c using the LASS spectrometer. The goal of this new experiment is to bring the data in both the inelastic and elastic channels, on K^* (e.g., $\bar{s}u$ states), and ϕ^* ($s\bar{s}$ states) up to the standard of the data used to understand the N^* and Y^* baryons and to make an order of magnitude increase in data on strangeness -2 and -3 hyperons. The existence of clean, radio-frequency

separated K^\pm beams, a 4π spectrometer with well-matched data processing power, and sophisticated phenomenological analysis programs provides a unique opportunity to understand the spectroscopy of the K^* , ϕ^* , Ξ^* , and Ω^* states. In a 1500-hour run at 180 pps equivalent, we expect to obtain a sensitivity of ~ 4 events/nb in the K^- and ~ 1 event/nb in the K^+ channels, with essentially uniform acceptance in all kinematic variables.

4. Equipment Required for the Experiment

- LASS spectrometer, including the new proportional detector system and the on-line data acquisition system.
- 34" liquid hydrogen target.
- RF separated beam line 20-21 providing $8K^-$ / pulse at 11 GeV/c.
- 9 processor 168/E data analysis system.

5. Estimate of Time Requirements

- 1500 hours (180 pps equivalent) data taking. In addition, we will require ~ 2 weeks of low repetition rate running at the beginning of each data-taking cycle to check and align the apparatus.

6. Data Analysis

- (a) On-line: We will require the LASS on-line data acquisition system for data logging, equipment checkout, and monitoring. For efficient use of beam time, this system will require the use of two 6250 BPI tape drives and the usual on-line support during the period of experimental data taking.
- (b) Off-line: Reconstruction of the data will require approximately one calendar year's usage of the 9-unit 168/E multiprocessor system with its associated Triplex support. Large-scale Monte Carlo studies will

also use the 168/E system. The physics analysis will be shared between the SLAC Triplex and the computers at INS and Nagoya, Japan.

I. INTRODUCTION

The last few years have been exciting ones in high energy physics. Since November 1974, we have seen a wealth of new experimental phenomena (ψ , D , T , etc.) coupled with theoretical developments which appear to explain the general trend of these discoveries rather well. Perhaps the most exciting of these theoretical developments is the emergence of what may be a theory of the strong interactions (QCD). Even though a complete theory of the hadron bound states has yet to be constructed, "atomic" quark models based on QCD and phenomenology have been very successful in explaining the level structure of heavy quark bound states. These models contain the basic SU(3) classification scheme of "light" quark (u, d, s) hadrons--now fifteen years old--which has been so successful in explaining and predicting many properties of the hadronic spectrum.

In spite of the successes of the theory, it is nevertheless true that many of the expected states have not yet been observed, even in the low-lying multiplets. This is the case for the meson spectrum in general; apart from the three established nonets 0^- , 1^- , 2^+ , most of the expected $I=0$ states have not yet been found, and many states (including K^*) of the $L=2$ supermultiplets are unobserved or not well established. Even less well known are the spectra of baryons with more than one strange quark, and mesons with $s\bar{s}$ content (the strange analogue of charmonium). In particular, only 3 of 16 Ξ^* and 0 of 7 Ω^* states are well established in the otherwise clearly defined baryon supermultiplets; and the ϕ meson (ground state of strangeonium) and the f' are the only $s\bar{s}$ states about which much is known. The fundamental experimental reason for this state of affairs is clear; nature has provided us with no stable meson or hyperon targets, so

that such states can be studied only in production experiments.

Aside from problems of the discovery and assignment of states within the quark model, many interesting questions are raised by QCD motivated models which have, as yet, no satisfactory answer. Drell-Yan processes and e^+e^- collisions are good probes for $J^{PC} 1^{--}$ systems, but the study of L dependence in $q\bar{q}$ systems and the radial spectrum for other than S-wave $q\bar{q}$ systems will depend heavily upon other kinds of experiments. At present only a study of light quark spectroscopy can confront these questions. The pattern of mass splittings of the $s\bar{s}$ and ($s\bar{u}$, $s\bar{d}$, $\bar{s}u$, $\bar{s}d$) spectroscopy contains important information about quark forces; any potential model of the $q\bar{q}$ interaction should make predictions concerning the level separation due to radial and orbital excitation as well as the splitting within a given level due to spin-orbit interaction [1]. We still do not know how good is the approximation of linear trajectories for L-excitations or how the widths of the states vary along such trajectories. If, as seems possible, high spin states decay via pionic cascades, not only high sensitivity but also an ability to deal with high multiplicity states will be required. The same remarks also apply to the underlying "daughter" states, and in addition a comparison of widths with the parent states is also interesting. We also need to know if the number of such daughters is as predicted by the quark model or is much larger as, for example, in the Veneziano scheme. There is now some understanding of heavy quarkonia but little information on the analogous light quark systems. A comparison of mass splittings in the $q\bar{q}$ systems containing u, d, and s quarks together with the information presently available on $c\bar{c}$ and $b\bar{b}$ may give useful insight into flavor dependence.

We must test the quark model rigorously; other states may exist with exotic quantum numbers or $qq\bar{q}\bar{q}$ content, and the "glueballs" required by QCD may also lie

among the ordinary mesons at low mass [2].

Thus we see that many interesting questions concerning the quark model remain unanswered; some were first asked many years ago, and some arise from the most recent attempts to understand inter-quark forces. We feel that our proposed experiment would effectively confront many of these issues. Below we discuss the size and timescale of the proposal before covering in more detail a selection of the many interesting topics.

I-2. Size and Timescale of the Proposed Experiment

We began the process of answering some of the above questions with two previous experiments, E-75 and E-132. E-75 was a 13 GeV/c K^+ experiment which used a forward dipole spectrometer in an RF separated beam line at SLAC. This experiment was very successful in studying the low mass, low multiplicity states. For example, we observed the $2\ 1^+$ Q mesons required by the quark model through a partial wave analysis of the $K\pi$ system. However, forward dipole experiments have serious difficulties in studying high mass or high spin states due to acceptance limitations for high mass and for high multiplicity states. We have therefore continued these studies in our current experiment (E-132), which makes use of the LASS spectrometer in a study of K^-p interactions at 11 GeV/c. This experiment has a sensitivity of ~ 700 events/ μb which is about ten times the statistical significance of the largest hydrogen bubble chamber experiments (see Fig. 1). When one considers the data on $K\pi$ elastic scattering it is of about the same sensitivity as the classic CERN-MUNICH study of $\pi-\pi$ scattering (see Fig. 2). In other words, by current standards this is a very large experiment, the state-of-the-art for studies of strange meson spectroscopy!

However, let us compare the sensitivity level of this experiment with that of the πN and $\bar{K}N$ scattering experiments which provided the data for the systematic study of baryon spectroscopy which is the basis for much of our confidence in the quark model classification scheme. The major breakthrough occurred when systematic analysis techniques were applied to rather complete sets of data. In the case of nucleon spectroscopy, by the late 1960's there were sufficiently good data for Lovelace and Donnachie [3] to understand not only the leading, but many of the underlying N^* states. The data involved good total cross section measurements every 10-20 MeV in the center of mass energy, elastic and charge exchange differential cross sections, and some good polarization data. In addition, good experiments on the inelastic scattering processes allowed the uncovering of new highly-inelastic states, and the systematic measurement of resonance couplings which resolved many of the ambiguities in classification of the N^* states. A similar story is true for the Y^* states. Fig. 2 also shows the sensitivity of these experiments. The elastic scattering studies are characterized by effective luminosities of 10,000-20,000 events/mb/20 MeV interval in the πN or $\bar{K}N$ center of mass energy. The studies of the inelastic final states were pursued at a level of $\sim 1,000$ events/mb/20 MeV.

We thus see that E-132 is about an order of magnitude down in sensitivity when compared to inelastic N^* and Y^* studies, and much more when contrasted with elastic πN and $\bar{K}N$ experiments. This order of magnitude is likely to be essential in gaining a good understanding of strange meson spectroscopy. Our proposed K^+ experiment, having a total sensitivity of ~ 5 events/nb would allow a study of $K\pi$ scattering in elastic and inelastic final states at the required effective luminosity of $\sim 1,000$ events/mb/20 MeV. As a production experiment for Ξ^* and Ω^* states

a K^-p sensitivity of ~ 4 events/nb would exceed the largest bubble chamber experiment by a factor of 30.

The existence of high energy RF separated beams at SLAC together with the $\sim 4\pi$ solid angle and high data rate capability of the LASS spectrometer provides a unique opportunity to make a significant advance in our understanding of the K^* , ϕ^* , Ξ^* , and Ω^* systems. We began this process with E-132, from which first results are now beginning to emerge; these will be discussed below. We are proposing a sequel experiment, also at 11 GeV/c incident momentum, which will study both K^-p and K^+p interactions at sensitivities of ~ 4 and ~ 1 event/nb respectively. The proposed timescale for this experiment is shown in Fig. 3, and there is seen to be little conflict with the completion of E-132. It should be noted that the short time for bulk data analysis is made possible only by the existence of the 168/E processor described in Appendix I.

In the following subsections we address in more detail a few of the many topics of interest which this experiment would enable us to study.

I-3. Production of $S = \pm 1$ Mesons

The primary goals of meson spectroscopy are the identification of particle states and the measurement of their properties, in particular mass and quantum numbers. The present status of strange meson spectroscopy is summarized in the quark model level diagram of Fig. 4; those states for which there exists experimental evidence are represented by solid lines. All of the states in Fig. 4 would be expected to lie in the mass region below ~ 2.5 GeV, and consequently should be accessible to our proposed experiment. We feel strongly that in attempting to detect and identify such states we need to make use of the comparison of K^+ - and K^- -induced reactions. This was important, for example, in understanding the $1^+ K\pi\pi$ amplitude in the E-75 analysis of the Q region

since the Deck background amplitude which interferes with the Q resonances is different for incident K^- than for incident K^+ .

Production of $K\pi$ states can be studied through reactions (1)-(8).



In experiment E-75 analysis of reactions (1)-(4) above a $K\pi$ mass of $1.5 \text{ GeV}/c^2$ was complicated by lack of acceptance and a four-fold ambiguity in the S-wave $K\pi$ phase shift. This could be resolved by study of reaction (6), which is accessible in the present proposal; (5) would also resolve the ambiguity but is made difficult by need to detect the π^0 . Even if E-132 confirms the $J^P = 1^- K^*$ (1700) found by E-75, corroboration from reactions (3) and (6) in the new experiment would be desirable.

Whereas the $K\pi$ states yield information only on natural parity K^* 's, $K\pi\pi$

states may result also from unnatural parity sources. Partial wave analysis

of reactions $K^- p \rightarrow K^- \pi^+ \pi^- p$ ----- (9)

and $K^+ p \rightarrow K^+ \pi^+ \pi^- p$ -----(10)

will continue to be useful in the L region and above (confirmation of $J^P = 2^-$ and 3^+ excited states). Large data samples from the reactions

$$K^- p \rightarrow K^- K^+ K^- p \quad \text{-----}(11)$$

$$K^+ p \rightarrow K^+ K^+ K^- p \quad \text{-----}(12)$$

should provide a complementary view of this mass region with a very different threshold. Data on the reactions

$$K^- p \rightarrow K_S^0 \pi^+ \pi^- n \quad \text{-----}(13)$$

$$K^+ p \rightarrow K_S^0 \pi^+ \pi^+ n \quad \text{-----}(14)$$

$$K^- p \rightarrow K_S^0 \pi^- \pi^- \Delta^{++} \quad \text{-----}(15)$$

$$K^+ p \rightarrow K_S^0 \pi^+ \pi^- \Delta^{++} \quad \text{-----}(16)$$

enable the study of charge exchange production of $K\pi\pi$ systems. In particular, reactions (13) and (16) should yield $J^P = 3^-, 4^+, 5^-$, etc. K^* 's, while (14) and (15) shed light on exotic $I = 3/2 K^*$ states.

The elasticity of known K^* states is observed to decrease with increasing mass, so that high-mass K^* 's should couple strongly to higher multiplicity $K-\pi$ systems. The LASS spectrometer is well suited to the bias-free detection of such systems and if, as expected, these states decay in a cascade mode, their existence, and possibly their quantum numbers, may be established by means of appropriate cuts on sub-system effective mass. Such a procedure would require large statistics in such channels, and clearly it would be desirable to observe the same structures in K^+ - and K^- - induced final states separately. This method is restricted to states with at most one π^0 . However, it may be extended to multi- π^0 states by

studying inclusive reactions such as

$$K^+_{p \rightarrow \Delta^{++}} (X)^0 \quad \text{-----} (17)$$

$$K^+_{p \rightarrow p} (X)^+ \quad \text{-----} (18)$$

$$K^-_{p \rightarrow p} (X)^- \quad \text{-----} (19)$$

$$K^-_{p \rightarrow \Delta^{++}} (X)^{-} \quad \text{-----} (20)$$

where X denotes the undetected $S = \frac{1}{2}$ system.

Given high enough statistics, the missing mass spectra may yield evidence for the existence of high mass K^* 's, especially as high multiplicity selections are made. For reactions (18) and (19) the proton would have to be identified. The present TOF system will allow this for high M_X , which is precisely the region of greatest interest. Reaction (20) is again a probe for $I = 3/2$ K^* states.

I-4. Strangeonium States

The ϕ is known as an almost pure $s\bar{s}$ state because of ideal mixing of the 1^- octet and singlet, and is the strangeonium analogue of the ψ . It is unfortunate that, with the rapid progress of charmonium spectroscopy in the last five years, strangeonium has been left far behind. The similarity of mass splittings among the $c\bar{c}$ and $b\bar{b}$ states encourages us to try to compare the mass splittings and transition scheme of $s\bar{s}$ states.

In the standard classification of mesons the radial excitations of the ϕ (analogues of ψ' , ψ'' , . . .) and also the L-excitations of the ϕ and f' are still missing. Recent e^+e^- data from ADONE and DCI, and photoproduction data from CERN OMEGA, show that the mass region above 1.3 GeV may be rich in such states. In addition the BNL-MPS $\pi^- p \rightarrow \phi \phi n$ experiment shows an excessive $\phi\phi$ yield compared with that expected from double suppression by the OZI rule. The existence of

heavy $s\bar{s}$ states may be indicated; production in $\pi^- p$ is strongly suppressed but decay into $\phi\phi$ is OZI allowed.

Hypercharge exchange with a K^- beam is a much better source of $s\bar{s}$ states than are the OZI-forbidden πp or pp interactions. The high statistics of the proposed experiment and its good efficiency for detection of recoil Λ^0 allow us to study various decay modes of the ϕ and f' and to make a sensitive search for related heavy $s\bar{s}$ states. The polarization measurement made by observing the $\Lambda^0 \rightarrow p\pi^-$ decay will also add to our knowledge of the production mechanism of such states. In view of the many possible decay modes of high mass $s\bar{s}$ states the ability to deal with high multiplicity may well be important (cf. the ρ').

I-5. Ξ^* and Ω^* States

Because they can be observed only in production experiments, and their decay topologies are complex, Ξ^* and Ω states have until recently only been studied in bubble chambers. Hyperon beams, particularly at the CERN SPS, have enabled high statistics studies of Ξ^- and Ω^- decays, but knowledge of their excited states remains poor.

Of the well established baryon supermultiplets $[56, 0^+]$, $[70, 1^-]$, $[56, 2^+]$, and $[56, 0^+]$, only the $[56, 0^+]$ is complete. No Ω^* states are known in the other supermultiplets, and although tentative evidence exists for several other Ξ^* states, only two, $\Xi(1820)$ and $\Xi(2030)$, are well established, and only tentative assignments to multiplets can be made. The fundamental reason for this lack of information is that the largest bubble chamber experiments with sensitivities of ~ 100 events/ μb produce only a few thousand Ξ^- and of order one hundred Ω^- .

E-132 already sees cleanly the Ξ^- and its lowest excited states the Ξ^* (1530). With the statistics presently available we also see the Ω^- at the expected level in the $\Lambda^0 K^-$ decay mode (see section II below). Compared with a bubble chamber, the minimum decay length cut of 2 cm applied at each secondary vertex is a small relative loss ($\sim 15\%$); in studying the Ω^- we are able to detect only the ΛK^- decay, but the branching ratio is large ($\sim 67\%$). A conservative estimate is that the proposed experiment should yield $\sim 3,000 \Omega^-$ and up to 150,000 Ξ^- .

This large increase in statistics should be sufficient to confirm many Ξ^* states and indicate their spins and parities through decays to lower Ξ^* states. In addition, it represents the first real opportunity to search for excited Ω^* 's. Moreover, there is still much to be learned about even the well established states. For example, although the Ω^- spin is now known to be $\geq 3/2$, there is no measurement of its parity; assignment to the $[56, 0^+]$ $J^P = 3/2^+$ decuplet is made on the basis of convenience--no known property contradicts such assignment. We should be able to measure the parity by observation of $\Xi^* \rightarrow \Omega^- K$ decays.

I-6. Summary

The proposed experiment in LASS is of very high sensitivity. We expect to fill many of the gaps in our knowledge of light $q\bar{q}$ systems and therefore to confront many of the fundamental questions about inter-quark forces. This will be done with parallel approaches, for example, on $K(n\pi)$, $3K$, and hypercharge exchange reactions. In addition, at this level of sensitivity, we will open up for the first time the possibility of systematic study of the $S = -2$ and -3 baryon spectrum.

II. SPECTROMETER PERFORMANCE

The solenoidal geometry of LASS, which is essential to its large acceptance, introduces some rather subtle pattern recognition problems when one attempts spatial reconstruction of tracks. Examples of the problems typically encountered are demonstrated in Figs. 5 and 6 where a relatively complex event is depicted in its natural spatial projections. In Fig. 5 where the observer is looking upbeam, letters represent cylindrical chamber match points and numbers indicate match points in the solenoidal planes--a representation which already interprets the coordinates in a way that aids in track recognition. In the plan view projection (Fig. 6), dots represent individual wire plane coordinates and letters, once again, represent match points in the cylindrical chambers. Without lines interconnecting points along each orbit, the event degenerates into a visual jumble of coordinates. In order to reconstruct tracks from this jumble, sophisticated pattern recognition programs are needed. Though development continues, the programs are now rather well understood and are both efficient in reconstructing tracks and rapid in execution.

The success of the programs in reproducing inclusive spectra is shown in Fig. 7. The transverse and longitudinal momentum spectra are shown for 16 GeV/c incident π^- from the total interaction trigger of E-127. These data, corrected for acceptance and tracking losses, are compared with Hydrogen Bubble Chamber results. The agreement is excellent.

Figures 8 through 9 show a number of mass and missing mass distributions which are indicative of the resolution capabilities of LASS in E-127 and E-132. Because of the variety of measuring devices and the many ways in which they may

be deployed on any given track (depending on the location of the production or decay vertex), no simple set of parameters may be assigned to describe the general resolution properties of the spectrometer. A comparison of theoretical and observed resolutions can only be properly made by a Monte Carlo simulation of the process and its subsequent detection by an idealized modeling of the spectrometer. The data for the K_S^0 mass (from $K^- p \rightarrow K_S^0 \pi^- p$) shown in Fig. 8(a) have a FWHM of 16 MeV as expected in the E-132 proposal. The Λ^0 mass spectrum (Fig. 8(b)) from E^- decay is much narrower, its FWHM is only 8 MeV. The missing-mass-squared spectra for $K^- p \rightarrow K^- \pi^+ \pi^- p$ and $K^- p \rightarrow K_S^0 \pi^- p$ (Fig. 9(a) and (b)) are substantially less than m_π^2 in width and show the characteristic peaking at a slightly negative value. Figure 8(c) shows the mass spectrum for 2γ events from E-127 in which there is a clear, sharp signal at the π^0 mass (FWHM 24 MeV). Finally, in Fig. 9(c) we see the missing-mass-squared recoiling against three prong events which are consistent with being a $K\pi\pi$ forward system. There is a clear peak at the nucleon mass with a FWHM of 0.4 GeV^2 .

The spectrometer has been used to study several exclusive channels thus far-- one two-body channel with large statistics and several multibody channels with substantially lower statistics.

The data shown in Fig 10 and 11 have been drawn from the primary trigger sample of E-132 using a software filter and processed all the way through the LASS analysis codes. From this data sample we have $\sim 100,000$ events of the reaction $K^- p \rightarrow K^- \pi^+ n$. The effective mass spectrum of the $K^- \pi^+$ system is shown in Fig. 10. There is good agreement, both in the absolute normalization and in the detailed structure of the $K^- \pi^+$ angular distribution, between our experiment, E-75 and the published bubble chamber data in the regions where the latter have

good statistics. Figure 11 is a three-dimensional scatter plot of the $K^- \pi^+$ effective mass and the cosine of the $K^- \pi^+$ scattering angle and shows the rich structure observed in the $K^- \pi^+$ elastic scattering reaction.

Only a small sample of data ($\sim 5\%$) from E-132 has been thus far fully processed without any software filter preselection. With this sample we have studied 3 or 4 prong and 1 or 2 prong + V^0 topologies to isolate the channels $K^- \pi^+ \pi^- p$ and $K_S^0 \pi^- p$.

We isolate the first channel by requiring that at least one negative be identified in the Čerenkov counters and that the overall information be consistent with the $K^- \pi^+ \pi^- p$ hypothesis. The final sample, in the four prong case, is selected by cuts on the missing-mass-squared distribution of Fig. 9(a) and on momentum balance. Similarly, three prong events are included in the sample if the recoiling mass is within the proton peak of Fig. 9(c). In Fig. 12 is shown the $K^- \pi^+ \pi^-$ mass spectrum for this channel with events in the $\Delta(1232)$ region excluded. Bubble chamber data at 10 GeV/c are included for comparison [4]; clearly (unlike forward dipole spectrometers such as E-75) there is no serious acceptance loss at high $K\pi\pi$ mass.

Looking in more detail at the Q region ($1.15 < M(K\pi\pi) < 1.4$), the raw distribution of the angle α in the $K^*\pi$ decay (see Fig. 13(a) for explanation) is shown in Fig. 13(b). For comparison, the raw and corrected distributions of E-75 in $1.28 < M(K\pi\pi) < 1.32$ are shown in Fig. 3(c) and (d). The $(1 + 4 \cos^2 \alpha)$ shape characteristic of the dominant $1+0+(K^*\pi)$ S wave is clearly seen, and the acceptance is clearly reasonably uniform.

Turning to the $K_S^0 \pi^- p$ channel, we see in Fig. 14, the π^+ decay distribution

in the K_S^0 rest frame. Apart from kinematic overlap with the Λ at $\cos \theta > 0.8$, it is flat. To identify the K_S^0 cleanly we exclude the Λ overlap region and apply a proper time τ cut $0.4 < \tau/\tau_{K^0} < 3.0$. Good events are then selected by making cuts on the missing-mass-squared distribution of Fig. 9(b) and on momentum balance. For the good 4C events, Fig. 15 shows the $K_S^0 \pi^-$ mass distribution. Clear K^* (891) and K^* (1430) signals are seen.

Within the present systematic uncertainties of the experiment (25%) we also understand the normalizations of these channels.

The spectrometer demonstrates a good ability to reconstruct Ξ^- if sufficiently restrictive cuts are made to insure the presence of a negative decaying track. With decay length cuts of 2 cm on the vertex separations, the $\Lambda \pi^-$ mass spectrum of Fig. 16 shows a clean Ξ^- at the correct mass with a FWHM 20 MeV. Combining these Ξ^- with π^+ from the main vertex gives the mass distribution of Fig. 17 which shows a clear $\Xi^*(1530)$ signal. The decay topology of $\Omega^- \rightarrow \Lambda K^-$ is very similar to Ξ^- and indeed, after removing some Ξ^- background, the Ω^- can be seen at the expected level in Fig. 18.

Thus, in addition to performing well for peripherally produced meson systems, the spectrometer has demonstrated that it can also detect complicated baryon systems — a capability formerly possessed only by bubble chambers.

III. DESCRIPTION OF THE EXPERIMENT

III-1. Spectrometer

This experiment proposes to use the LASS spectrometer facility and the existing RF separated beam line. LASS contains two large magnets and associated detectors as shown in Fig. 19. The first magnet is a superconducting solenoid of 23 kG field with the field direction parallel to the beam direction. This is followed by a 30 kG meter dipole magnet with a vertical field. Particle identification is provided by \check{C}_1 and \check{C}_2 and a time-of-flight (TOF) hodoscope. Several proportional wire chambers (PWC) and scintillation counter hodoscopes provide in time spatial information and, in addition, a variety of trigger capabilities. A series of conventional magnetostrictive spark chambers provides track information upstream and downstream of the dipole. Within the solenoid, track information is provided entirely by proportional chambers. A complete description of the LASS spectrometer is given in the appendix of SLAC Proposal E-109 with further details available in SLAC Proposal E-132. The principal change made since that time is the replacement of all spark chambers in the solenoid with proportional chambers. In the following sub-sections we will review briefly the major components of the spectrometer, paying particular attention to those portions of the apparatus which differ from those described in our previous documentation.

III-1.1. Solenoid

Figure 20 is a detailed schematic of the detectors within the solenoid. The PWC plug chambers, the trigger/track chambers, and the full bore chambers remain unchanged. Each plug chamber has three planes of anode readout having 1 mm wire spacing and covering an area 256 mm square centered on the beam axis. Each of the

trigger/track chambers has one wire plane with the wires spaced 4 mm apart. One cathode of each chamber is etched to form two concentric rings of 128 sectors. The 256 pads so formed, when read out, give 2.8° angular resolution. Each full bore chamber consists of three proportional planes of 640 wires, with 2 mm wire spacing.

A new vertex detector package has been developed for LASS by Carleton University. The package consists of a set of six concentric cylindrical proportional chambers surrounding the 34" LH_2 target cell. Each chamber has a set of anode wires with 2 mm spacing which run parallel to the beam axis. The cathodes consist of 7 mm etched strips at $\pm 10^\circ$ to the anode wires. The chamber construction technique of using Hexcel paper honeycomb sandwiched between aluminum mylar laminate results in a chamber thickness of approximately 0.11 gm/cm^2 . The radii of the anode cylinders are approximately 6, 9.5, 13, 16.5, 30, 50 cm, and the anode to cathode spacing is approximately 5 mm.

Signals are taken from both the anode and the cathodes. The anode wires are read out using our conventional electronics, and provide the fast timing information. The pulse heights from the cathode strips are analyzed by a modification of the SLAC SHAM/BADC system (SHAM IV). The distribution of pulse heights in neighboring strips will then result in a spatial resolution of $\sim .5 \text{ mm}$.

A new series of planar proportional chambers has also been developed to replace the C-D spark chambers presently in use in the intercoil gaps of the solenoid. These new GAP chambers will have a sense wire plane with 2 mm wire spacing and the two cathodes will have etched strips at $\pm 45^\circ$ to the sense wires. The anode to cathode gap will be 5 mm, and each plane will have 768 wires. A region of

approximately 8 cm radius centered on the beam axis will be deadened by the inclusion of a polyurethane plug. These chambers will provide both anode and cathode readout and the fast timing information and spatial resolution already discussed.

The primary advantage of this all-proportional solenoid over the earlier system is the large reduction in the random background rate. This will reduce the time required to process events while also reducing the confusion caused by multiple hits. At the same time, the data taking rate will be increased, since the beam flux can be raised and the triggering deadtime lowered. The improved spatial resolution of the new cylindrical package will improve the momentum resolution for the large angle slow recoils. Finally, the higher efficiencies will simplify the tracking algorithms, thus decreasing the time required to process events and allowing reliable reconstruction of short tracks.

III-1-2. Dipole Spectrometer

Located downstream of the solenoid is a conventional spark chamber-dipole-spark chamber spectrometer. All C-D chambers in this system have been replaced by magnetostrictive chambers. In front of the magnet there are three 2 gap spark chamber modules with a total lever arm of 1.0 m. There are also two 4 mm wire spacing proportional chamber hodoscopes to provide timing information for track identification. Immediately downstream of the magnet there are a PWC hodoscope, the downstream spark chamber package consisting of four 2 gap modules, and two counter hodoscopes to provide timing information. The momentum acceptance of this package has been extended downward somewhat by rearranging the chambers so that the larger chambers are now

behind the dipole.

III-1.3. Particle Identification

Particle identification is provided by Č1, a 38 element atmospheric pressure threshold Čerenkov hodoscope at the end of the solenoid; by Č2, an 8 element pressurized threshold Čerenkov counter following the dipole spectrometer; and by a 24 element time-of-flight (TOF) hodoscope located just downstream of Č1 (see Fig. 19). Č1 will be filled with Fr-114 which provides π/K separation between 3.0 and 11 GeV/c. Č2 will be filled with Fr-12 at 1.25 atmospheres so that it will overlap Č1 in the critical forward region where Č1 has a hole. The TOF hodoscope provides K/π separation up to 1.3 GeV/c, K/p separation up to 2.1 GeV/c, and π/p separation up to 2.5 GeV/c.

III-1-4. Beam

Minor changes have been made to the beam-defining scintillation counters, reducing their thickness, and increasing their efficiency. A more consistent technique for tagging multiple incident beam particles has been implemented as well.

A more fundamental change is under consideration. In an attempt to match the inherent time resolution of the PWC chambers to the characteristics of the beam, we plan to restructure the 1.5 μ s SLAC beam spill into fifteen 10 ns buckets spaced at 100 ns intervals. It should then be possible to unambiguously eliminate all random background in the solenoid for a well defined fraction of the beam (typically > 90%). On the basis of our present knowledge, we believe the required beam currents should be attainable in this operations mode. However, tests will be made during the next cycle to determine the beam fluxes that can be reached.

III-2. The LASS Multi-Processor System

The LASS multiprocessor system must be regarded as an integral part of the experimental hardware, since the data from an experiment of this size could not be reconstructed within the normal constraints of time availability on central computing facilities. Therefore, we will here describe the basic architecture of the processor system, paying particular attention to its performance.

More details concerning the hardware of the processors are available in Appendix I. A brief review of the net impact of these devices on the reconstruction of the data from this proposal is given in section III-5.

III-2-1. 168/E Processors

The 168/E micro-processors are the result of development efforts to provide substantial computer analysis power to handle the data processing load from LASS. They have been designed to emulate the subset of instructions of an IBM 360/370 computer required by a standard scientific FORTRAN program. The goal is to be able to run the track finding and fitting programs interchangeably on the main computer or on the emulator. The full diagnostic power, and utility program resources, of the main center are then available to check and exploit the emulator.

Initially there will be a system of six 168/E processors, to be increased to nine by spring of 1980. The equivalent processing power of each unit is equal to one half of an entire 370/168. The overhead on the main computer to oversee, feed, and drive the emulator system has been measured at 3.6 msec/event or $\sim 2\%$ of a 370/168 for our system of six processors.

The cost of the system is decreasing rapidly with the cost of memory, but at present each processor costs about \$15,000 and is driven by a controller-buffer

memory complex (called the "Bermuda Triangle") which costs about \$30,000. A single controller can handle up to nine processors without serious loss of performance. (The nine actually become 8.2 effective processors.)

The processors have been tested and shown to work as expected by running the main segments of LASS code, the full event reconstruction code from the TASSO Group at DESY, several CERN codes, and the fast trigger programs from the SLAC Bubble Chamber group.

The system is in the final stages of debugging. The controller has been operational for five months, and the "Bermuda Triangle" hardware is installed and checked out. The software system to handle feeding data from the IBM host to the processors and to execute a program of multiple overlays is being tested. Our schedule shows us in production with one processor in October, the second running in November, six by the end of the year, and the final three by April 1980.

III-2-2. System Performance

Based on the tests with the LASS codes, TASSO codes, etc., a 168/E processor performs at slightly more than one half a 370/168 equivalent depending upon the instruction mix. Hence, if the estimated processing time per event is 0.5 sec on the 370/168, it will be ~ 1 sec on the 168/E. There is a further 10% overhead for loading the overlay segments into the program memory (128K of micro-instructions requires about 90 msec to load). If we fold these figures with typically 22 hours/day of scheduled operations and 10% unscheduled outage on the triplex, each 168/E processor should deliver 300 CPU hours equivalent per month. In terms of SLAC's current charging scheme, this represents 2.4×10^6 CU's per month per 168/E.

We feel we can install all nine processors on one system without seriously degrading their performance, thus delivering 2500 370/168 CPU hours equivalent

per month for reducing these data or $\sim 20 \times 10^6$ CU's of computing.

III-3. Trigger

The physics topics of interest in this experiment span the range of ~~the~~ charged particle topologies. Moreover, the experimental data must be bias-free over the entire phase space of the many different channels. These considerations imply that the trigger cross section must be a relatively large fraction of σ_{tot} . Conversely, "extra" triggers increase the deadtime and lead to a lower integrated sensitivity. Moreover, useless triggers increase the event reconstruction time per good event. Thus, it is important to try to eliminate triggers from trivial sources (such as K decay, interactions outside the hydrogen) and from large cross section channels which are well measured (such as small t elastic Kp scattering). The simplest implementation of these considerations leads naturally to a trigger based on counting the number of tracks leaving the target region.

Such a trigger can be implemented in LASS in several different ways. In E-132, for example, the trigger required \geq two hits in the PWC 1.5, \geq one hit in the TOF, and no hit in the beam veto counter (LP3) located behind the dipole. This trigger led to a triggering cross section for an incident K^- beam of 20.5 mb with a 4.7 mb empty target rate. The ~ 16 mb triggering rate of LH_2 includes essentially all of the \geq four prong channels plus most of the interesting two prong and two prong + V^0 data. Most of the forward elastic and the two prong proton diffraction dissociation data are effectively suppressed. Offline studies of E-132 data have indicated that the empty target rate can be greatly reduced by adding additional PWC chambers to the multiplicity definition and tightening the timing on the TOF hodoscope to reduce the random rate. This leads to a trigger rate for the proposed experiment of .06 of the beam

rate or an effective trigger cross section of 16.7 mb. The K^+ trigger rate will be $\sim 20\%$ less.

The primary improvement which can be made in this trigger is to improve its uniformity for the two prongs. In particular, at high mass ($m_{K\pi} > 2.4$ GeV) the asymmetric regions are lost from the trigger because the slow particle runs into the solenoid wall before reaching PWC 1.5. The new vertex detectors allow us to eliminate this trigger acceptance loss by replacing the PWC 1.5 multiplicity part of the logic with a multiplicity box surrounding the target made up of cylindrical plus plug proportional chamber. The basic trigger will thus require ≥ 2 hits in cylinder 1 + plug 1; ≥ 1 hit in the TOF; and no hit in the beam veto counter. Simulations of this trigger scheme using random beam triggers from E-132 indicate that rates will be comparable with those using the PWC 1.5 cluster logic. This basic trigger will be complemented by several other prescaled triggers to provide calibration and specific channel information.

The many digitized detectors present in LASS provide a facility for software selection of the data offline before final processing. These more specific triggers can use 1) scintillation counters and proportional chambers, 2) particle identification information, and 3) the three induced readout proportional chamber wheels which provide a direct measurement of the P_L and P_T of the outgoing secondary particles. As a simple example, a software filter using PWC and scintillation counter multiplicity information has been used in E-132 to select the $K\pi$ events from the data tapes before event reconstruction in order to allow the full statistics of the $K\pi$ data to be available rapidly.

III-4. Event Rates

Our expected event rates can be estimated reliably from the performance of our previous experiments. For example, estimates made for the E-132 proposal

from Monte Carlo studies and experience with E-75 have been shown to be correct within 25%. Using this same procedure we have derived estimates for this proposal based on results from E-127 and E-132. We have assumed a beam flux of $8K^-$ per pulse at 120 pps, beam track reconstruction efficiency of 86% including absorption and decay, data taking efficiency of 75%, a triggering efficiency of 94%, and an event deadtime of 16ms. The measured reconstruction efficiency in a clean environment is 97%; absorption and decay are typically 6% per track. For a typical 4 prong reaction, acceptance (including particle identification) efficiency is about 75%. We find that a 1,500 hour experiment at 180 pps equivalent corresponds to a total reconstructed data sample of ~ 5 events/nb. It is intended to divide this between K^+ and K^- running in the ratio 1:4.

In Table I we summarize some cross sections and the total number of events expected for several specific K^\pm channels. Note that large samples exist even for reactions with low cross sections. For example, the sample should contain $\sim 3,000 \Omega^-$ events.

III-5. Data Reduction

III-5.1. Data Acquisition

The LASS Data acquisition system utilizes a PDP-11/10 to pass data from the individual LASS detectors to the SLAC triplex system via a high-speed data link. The data are recorded on the high density 6250 BPI tape drives of the triplex system while some fraction undergoes a complete analysis. For efficient use of beam, this system requires the use of two tape drives and normal on-line service during the period of experimental data taking. Experience with this system has shown it to be fully capable of handling the rather high data rates expected in this experiment as well as providing flexible and complete monitoring of the entire experimental apparatus.

III-5-2. Data Processing and Analysis

This experiment, during its full course, will collect approximately 180 million events which will require subsequent off-line reconstruction and analysis. The present LASS programs process E-132 data at a rate of 0.75 sec/event, and we estimate that, with the new spectrometer configuration (in which the solenoid contains fully proportional chambers), this figure will be reduced to ~ 0.5 sec/event. The total processing time is therefore ~ 3 CPU years.

It would clearly be impossible to deal with such a large amount of data processing within normal usage allocations of the central computing facility. For example, at our present usage rates, it would take us over ten calendar years to process this experiment on the SLAC triplex. However, using the nine 168/E processors which we are currently planning to build, this amount of computing can be comfortably delivered in one year of calendar time and will have only a small impact on the laboratory's conventional processors.

In addition to the basic reduction of the data, the 168/E's will also be used to run the Monte Carlo correction programs. However, we will require use of conventional processors for DST passes, angular momentum analyses, etc. There exists a full set of programs to complete the physics analysis of the two and three body meson states, and programs to handle states of higher multiplicity are currently under development. These programs have been developed for use in our previous experiments (E-75, E-127, and E-132) and are immediately applicable to the experiment proposed here. We would plan to perform this analysis using both the SLAC triplex and computers at INS and Nagoya. The Japanese portion of the collaboration has a total of ~ 100 hours/month equivalent

168 time available during the next year, and this allocation is expected to grow with time. With such a large sample of data in many different channels, it is difficult with any great precision to estimate the total amount of central computer time we will require. However, since we estimate that the physics analysis will be spread over approximately two years, we conclude that it can be accomplished within our present allocations.

III-6. Running Time

This proposal requires the equivalent of 1,500 hours of data taking at 180 pps. We plan to run this experiment at rather high kaon fluxes (8 K/pulse). This will require ~ 50 mA current from the linac at ~ 21 GeV primary energy. As part of the checkout of the new LASS solenoid detectors, we expect to set up the entire spectrometer at low repetition rates immediately prior to the beginning of this experiment, so little additional set-up time specific to this experiment will be required. One week at 10-20 pps should be sufficient to align the spectrometer, check the trigger, and verify the operation of the other LASS detectors and the K^{\pm} beam. If a significant interval of down time separates two periods of data taking, our previous experience indicates that a minimum of two weeks at low repetition rates will be required to attain a fully set up spectrometer. While a good part of the set-up can be done during SLED running, the data taking is not compatible with a SLED beam. We expect the proportional chamber modifications to LASS to be finished in March 1980 and would hope that this experiment, if approved, would begin data taking shortly thereafter.

IV. Summary

We propose to study K^+p and K^-p interactions at 11 GeV/c using the LASS

spectrometer. The goal of this new experiment is to bring the data, in both the inelastic and elastic channels, on K^* (e.g., $s\bar{u}$ states) and ϕ^* ($s\bar{s}$ states) up to the standard of the data used to understand the N^* and Y^* baryons and to make an order of magnitude improvement in the data on Ξ^* and Ω^* states. The existence of clean radio-frequency separated K^+ beams, a 4π spectrometer with well matched data processing power, and sophisticated phenomenological analysis programs should provide a unique opportunity to understand the spectroscopy of the K^* , ϕ^* , Ξ^* , and Ω^* states. In a 1,500-hour run at 180 pps equivalent, we expect to obtain a sensitivity of ~ 4 events/nb in the K^- and ~ 1 event/nb in the K^+ channels, with essentially uniform acceptance in all kinematic variables.

APPENDIX I

The LASS Multiprocessor System

The basic component of the multiprocessor is a microprocessor (168/E) which has been designed to emulate a major subset of the instructions of an IBM 370. This subset of executable instructions is chosen to encompass essentially all the machine instruction output from the standard 370 FORTRAN compiler. The goal is to be able to run the complete track reconstruction codes without a large increase in software effort and yet retain a fair degree of flexibility. The 168/E consists of five kinds of circuit board.

Appendix I-1. Integer CPU

The integer CPU circuit is based on the 2901, which is a LSI bit slice microprocessor chip introduced by Advanced Micro Devices in the summer of 1975. It has become the standard bit slice component with all but two of the bipolar semiconductor manufacturers producing it. This board handles the following types of IBM 360/370 instructions: 16-bit integer (INTEGER*2), 32-bit integer (INTEGER*4), 32-bit logical (LOGICAL*4), all conditional branching, and all memory addressing. It has a 150-nsec cycle time. The throughput on FORTRAN programs has been measured to be between 1.3 to 1.8 times slower than a 370/168 depending on the program instruction mix. The only noticeably slow instruction, when compared to the 370/168, is multiplication. A prototype wire-wrapped processor has been functioning since the summer of 1977. The final board will be an 8-layer printed circuit board costing \$600 including components and labor charge for assembly.

Appendix I-2. Floating Point

The floating point processor consists of two circuit boards. It is entirely MSI logic but uses the "new" MSI circuits which have been introduced

to support the LSI components. The processor handles all IBM 360/370 single precision floating point instructions with exactly the same results, bit for bit, as the 370/168 (the 360/91 may produce different results on division), but since the single precision format of IBM contains only a 24-bit mantissa, some form of extended precision is required for the LASS production code. For example, when calculating if two helices in the solenoid intersect, one would like to be able to calculate the distance of closest approach to a precision better than the resolution of the detectors. This precision is not possible with the IBM single precision format when the radii of curvature are large. It has been found experimentally that about eight more bits are required in the mantissa to perform the calculation with sufficient precision. On the 360/370, the important variables are declared REAL*8 which adds 32 additional bits to the mantissa. On the 168/E, we have made a compromise between true emulation and circuit cost and complexity. The floating point processor has pseudo-double precision instructions which add 16 bits to the mantissa. Thus the processor can do either 32-bit or 48-bit floating point arithmetic. The cycle time of the processor is either 100 or 150 nsec dependent on the instruction. It operates with an internal Read-Only-Memory (ROM) to control the steps in a floating point operation. This ROM could be considered as Nano-processor program memory. The speed of the processor is about a factor of two faster than most mini-computers and a factor of two slower than the 370/168. Again, multiplication is the slowest instruction. The circuit boards are eight-layer printed circuit boards. The cost of the floating point processor is \$1,200, including components and labor.

Appendix I-3. Memory

The memory for the 168/E is in two parts, one for the program and the other

for the data. Both are based on the Intel 2147 memory I.C. This circuit contains 4,096 words of one bit with a 70-nsec access and cycle time. It has a unique feature in that when the memory is not being addressed, it powers down to one-tenth of its normal operating current. Thus a processor with eight memory boards draws only as much power as one memory board plus seven-tenths of one memory board. Since each memory board draws about 25 watts, considerable power is saved in the system, and more importantly, there is considerably less generation of heat which is the major factor in I.C. component failure. The Intel 2147 has become the industrial standard circuit and although only Intel has large production experience now, several other companies have just announced that they are also producing it. The current list price is about \$25, when ordered in large quantities. The memory board is a four-layer printed circuit board with one half containing 32 memory circuits for data and the other half containing 24 memory circuits for program. That is, one memory board contains exactly 16 K bytes of data and 4096 micro-instructions which is about 8 K bytes of IBM object code or about 500 lines of FORTRAN. The cost of the board is \$1800, i.e., about \$50/KByte for data and \$75/KByte for program. By comparison, mini-computer add-in memory is commercially available for about \$30/KByte. The high cost of the memory for the 168/E arises because the high speed of the processor must be matched by the memory.

Appendix I-4. Interface

As the 168/E is not capable of performing any input or output instructions, it can talk only to its memory. The interface allows a real computer to load the memories with program and raw data, and to read the processed results. The interface is very simple. Either the processor or the interface controls the

memory and never both simultaneously. The interface control logic can shut off the processor so that it releases the memory busses. Then the interface can take the busses and control them.

Appendix I-5. "Bermuda Triangle" System

Since the track-finding code itself takes up most of the memory space capabilities of the 168/E, a system had to be designed to allow the 168/E memory to be overlaid so that the entire program could be executed by the processor. This system is called the "Bermuda Triangle." It consists of a large memory to hold a single copy of all the program to be executed. The memory used is slower but much less expensive than the 168/E memory. Two "Bermuda Triangles" are used, one for the program memory with 128K words of 24 bits, and one for the data memory with 192K bytes. A cable is used to transfer data from the memories to the processors. The transfer uses a protocol which is essentially identical to the one being developed by the FASTBUS committee. The controller for the transfer is a DMA in the Triangle. The rate of transfer on the FASTBUS is one word in 70 ns, thus the total time to overlay the 128K micro-instructions is 90 ms and the transfer rate on the data side is nearly six Mega Bytes per second.

Another leg of the Triangle is an interface between the UNIBUS of a PDP-11 and the FASTBUS. It is used to allow access to the processors from the PDP-11 to start the 168/E's and to read their status when they halt. Finally, the last leg is an interface between the UNIBUS and the buffer memory for purposes of loading the memories initially and reading and writing event data. The three interfaces are contained on one wire-wrapped card and all control functions are performed by the PDP-11.

The "Bermuda Triangle" was installed in late August 1979 and at this date the final changes are being made to the software in the PDP-11 control program.

The LASS track reconstruction code has been divided into nine overlays corresponding to nine logical steps in the code, such as unpacking the raw data, finding beam tracks, finding tracks downstream of the dipole, etc. With these overlays, the 168/E will do all of the first pass analysis from raw input data to final data summary tape formatting, including the code to monitor the efficiencies of the chambers, Čerenkov counters, etc.

Appendix I-6. Channel Interface

With the 168/E's and the "Bermuda Triangle," the PDP-11 only needs a source for the raw data and a sink for the results. For this purpose, an interface was designed between the UNIBUS and the Channel of the IBM 360/370 computer. It allows transfer of data between the 360/370 and the PDP-11 at full channel speeds (1.2 MB/s) with the minimum overhead on the IBM system. We have measured the CPU overhead on the 360/91 to be only 3.6 msec per event and we will soon cut it down by at least a factor of 2.

Thus the IBM 360/370 will be used to read the raw data from tape, send it to the PDP-11 to be processed by the 168/E - Bermuda Triangle system, and receive the DST results to be put on tape. The IBM system, already under 24-hour operation, handles all the job scheduling, tape mounting, etc. Production JOBS will be submitted to the system as before, and each JOB will first initialize the PDP-11 and buffer memories.

TABLE I

CROSS SECTION AND ESTIMATED NUMBER OF EVENTS
FOR SELECTED $K^\pm p$ REACTIONS

<u>Reaction</u>	<u>Cross section (μb)</u>	<u>Expected number of events</u>
<u>I. Inclusive Channels</u>		
$K^- p \rightarrow (K^0 + \bar{K}^0) X^0$	8260	14×10^6
$K^- p \rightarrow \Lambda^0 X^0$	2520	4×10^6
$K^- p \rightarrow \Xi^- X^+$	128	1.7×10^5
$K^- p \rightarrow \Omega^- X^+$	2.4	3000
$K^+ p \rightarrow K^0 X^{++}$	5800	2.4×10^6
$K^+ p \rightarrow \Lambda^0 X^{++}$	350	1.4×10^5
<u>II. Hypercharge Exchange Channels</u>		
$K^- p \rightarrow K^+ K^- \Lambda$	12	6.2×10^4
$K^- p \rightarrow \phi \Lambda$	7	3.6×10^4
$K^- p \rightarrow f' \Lambda$	2.5	1.3×10^4
$K^- p \rightarrow K_S^0 K^\pm \pi^\mp \Lambda$ $\quad \quad \quad \downarrow$ $\quad \quad \quad \rightarrow \pi^+ \pi^-$	4	1.8×10^4
$K^- p \rightarrow K^+ K^- \pi^+ \pi^- \Lambda$	10	4.7×10^4
$K^- p \rightarrow \pi^+ \pi^- \Lambda$	40	2.1×10^5
$K^- p \rightarrow \rho \Lambda$	10	5.1×10^4
$K^- p \rightarrow f \Lambda$	4	2.0×10^4
$K^+ p \rightarrow K^+ K^+ \Lambda$	12	1.5×10^4
$K^+ p \rightarrow K_S^0 K^+ \pi^+ \Lambda$ $\quad \quad \quad \downarrow$ $\quad \quad \quad \rightarrow \pi^+ \pi^-$	9	1.0×10^4

TABLE I (cont'd)

<u>Reaction</u>	<u>Cross Section (μb)</u>	<u>Expected number of events</u>
<u>III. K Channels</u>		
$\text{K}^- \text{p} \rightarrow \text{K}^- \pi^+ \text{n}$	350	1.8×10^6
$\text{K}^- \text{p} \rightarrow \text{K}^- \pi^+ \pi^- \text{p}$	850	4.3×10^6
$\text{K}^- \text{p} \rightarrow \text{"Q"} \text{P} (1.0 < M_{\text{K}\pi\pi} < 1.5 \text{ GeV})$	260	1.4×10^6
$\text{K}^- \text{p} \rightarrow \text{"L"} \text{P} (1.5 < M_{\text{K}\pi\pi} < 2 \text{ GeV})$	140	7.1×10^5
$\text{K}^- \text{p} \rightarrow \text{K}^- \text{K}^+ \text{K}^- \text{p}$	30	9.7×10^4
$\text{K}^+ \text{p} \rightarrow \text{K}^+ \pi^+ \text{n}$	~ 100	$\sim 1 \times 10^5$
$\text{K}^+ \text{p} \rightarrow \text{K}^+ \pi^+ \pi^- \text{p}$	1200	1.4×10^6
$\text{K}^+ \text{p} \rightarrow \text{K}^0 \pi^+ \pi^+ \text{n}$	180	6.8×10^5

12. $K^- \pi^+ \pi^-$ mass distribution from $K^- p \rightarrow K^- \pi^+ \pi^- p$ channel compared with bubble chamber data. Cuts $|t'_{p \rightarrow p}| < 1.0 \text{ GeV}^2$ and $m(p\pi) > 1.4 \text{ GeV}/c^2$ have been applied.
13. $K^- \pi^+ \pi^-$ decay angle $\alpha(K^*\pi)$ in "Q" region (a) definition; (b) E-132 raw data; (c) E-75 raw data; (d) E-75 data acceptance corrected.
14. $K_S^0 \rightarrow \pi^+ \pi^-$ center-of-mass decay angle $\cos \theta_H$.
15. $K_S^0 \pi^-$ mass distribution from $K^- p \rightarrow K_S^0 \pi^- p$.
16. $\Lambda^0 \pi^-$ mass distribution from V^- topology events.
17. $\Xi^- \pi^+$ mass distribution; Ξ^- from Fig. 16 combined with π^+ from main vertex.
18. $\Lambda^0 K^-$ mass distribution from V^- topology events. Ξ^- background has been removed.
19. Plan view of the LASS spectrometer.
20. Expanded plan view of the LASS solenoid.

REFERENCES

1. For example: H. S. Schnitzer, Phys. Rev. D13, 74 (1976).
2. For example: R. L. Jaffe and K. Johnson, Phys. Lett. 60B, 201 (1976).
R. L. Jaffe, Phys. Rev. D15, 267 (1977).
3. A. Donnachie, R. A. Kirsópp, C. Lovelace, Phys. Lett. 26B, 161 (1968).
4. A-B-B-C-H-L-V Collaboration, Nucl. Phys. B101, 304 (1975).

12. $K^- \pi^+ \pi^-$ mass distribution from $K^- p \rightarrow K^- \pi^+ \pi^- p$ channel compared with bubble chamber data. Cuts $|t'_{p \rightarrow p}| < 1.0 \text{ GeV}^2$ and $m(p\pi) > 1.4 \text{ GeV}/c^2$ have been applied.
13. $K^- \pi^+ \pi^-$ decay angle $\alpha(K^*\pi)$ in "Q" region (a) definition; (b) E-132 raw data; (c) E-75 raw data; (d) E-75 data acceptance corrected.
14. $K_S^0 \rightarrow \pi^+ \pi^-$ center-of-mass decay angle $\cos \theta_H$.
15. $K_S^0 \pi^-$ mass distribution from $K^- p \rightarrow K_S^0 \pi^- p$.
16. $\Lambda^0 \pi^-$ mass distribution from V^- topology events.
17. $E^- \pi^+$ mass distribution; E^- from Fig. 16 combined with π^+ from main vertex.
18. $\Lambda^0 K^-$ mass distribution from V^- topology events. E^- background has been removed.
19. Plan view of the LASS spectrometer.
10. Expanded plan view of the LASS solenoid.

EVENTS/ μ b

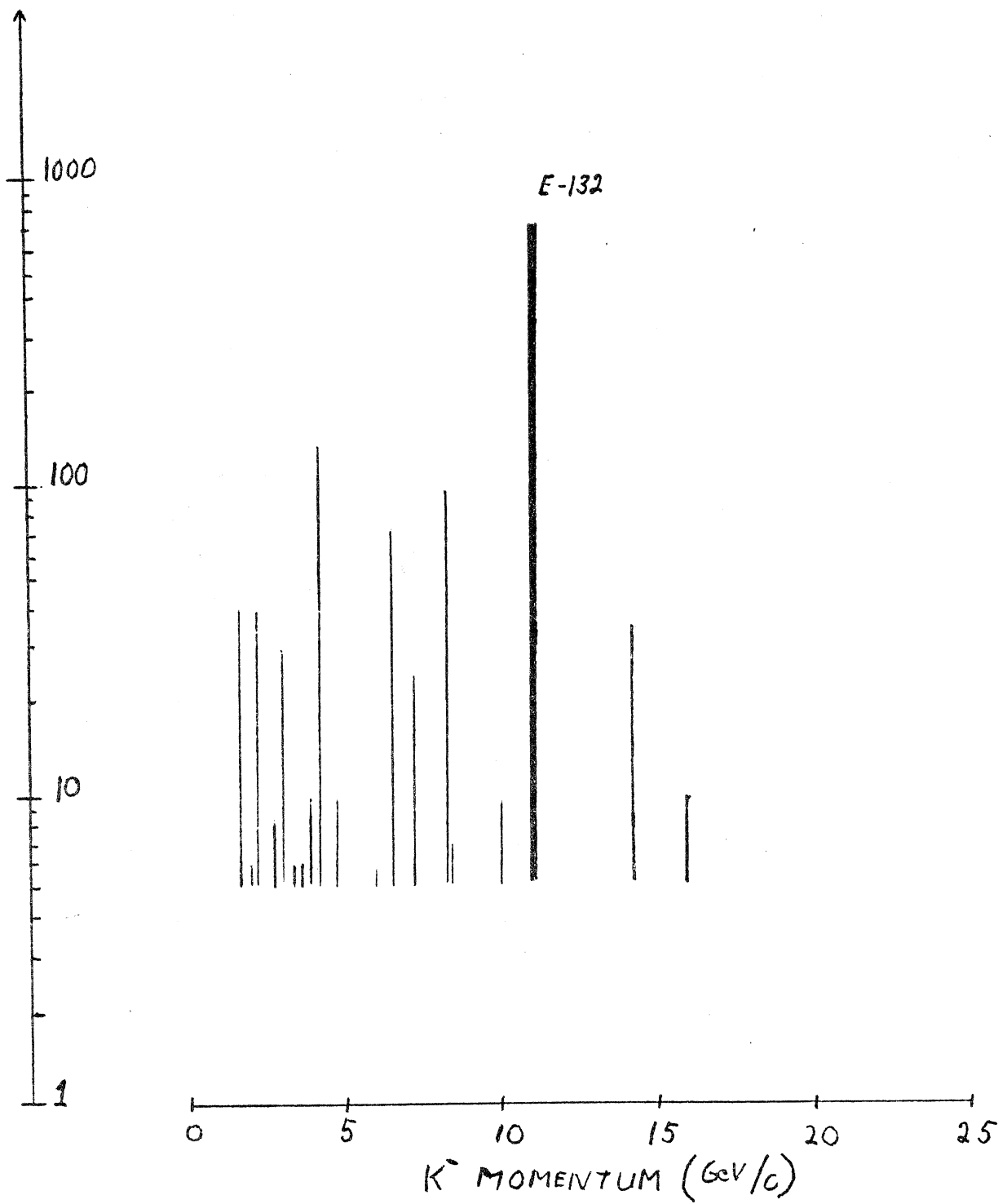


Fig. 1

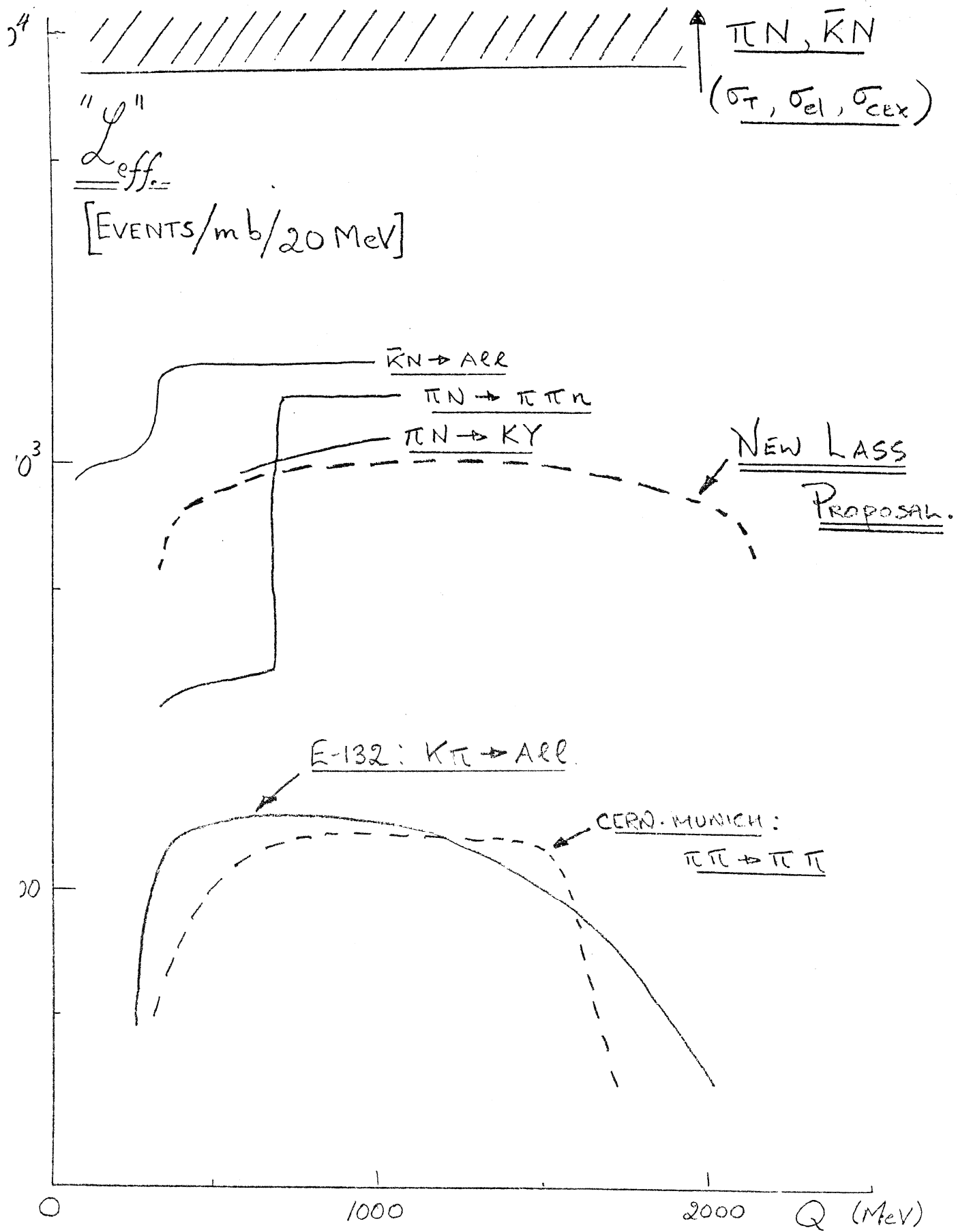


Fig. 2

A TIMETABLE FOR THE NEW EXPERIMENT

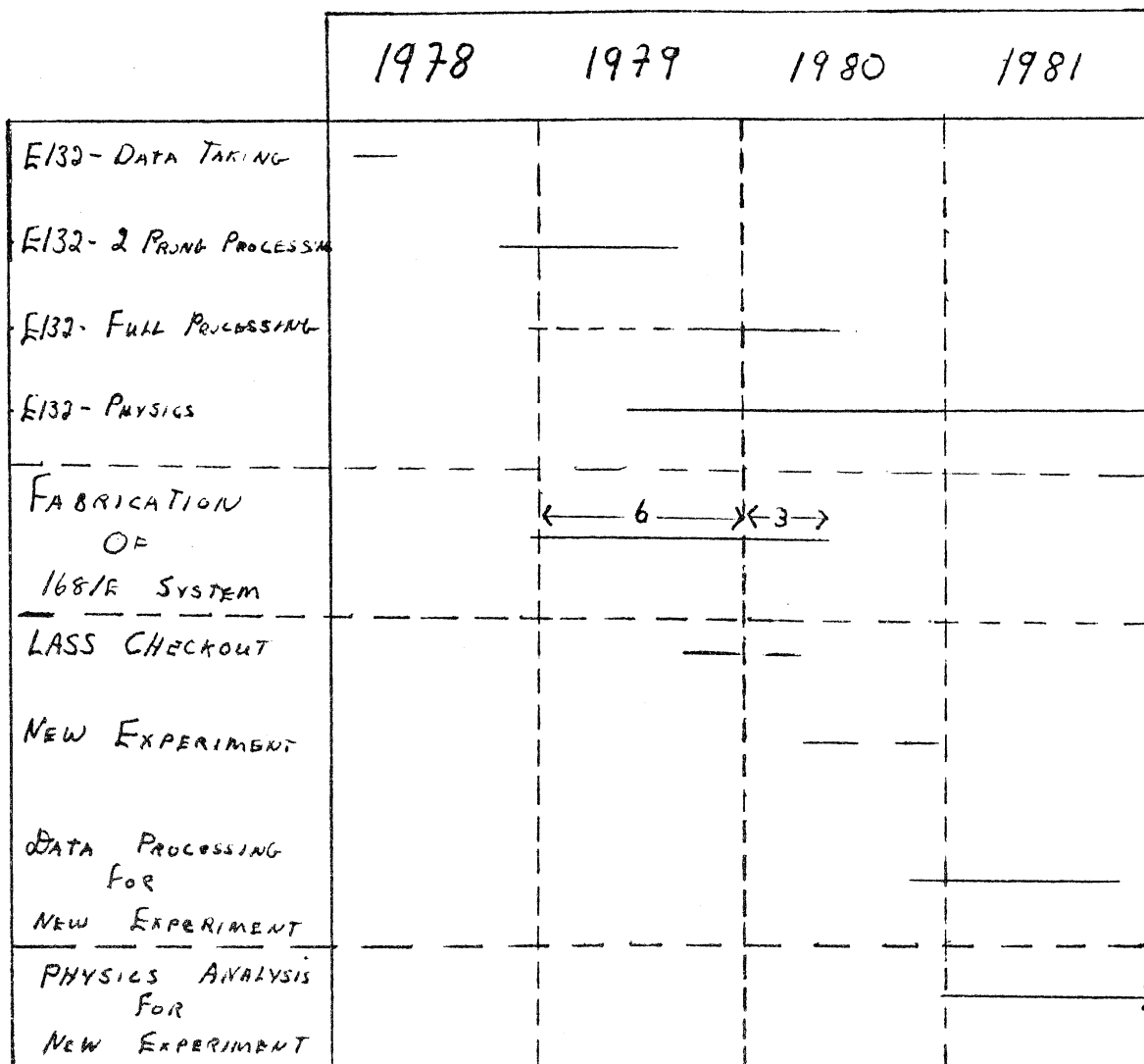
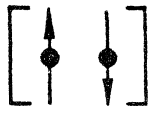
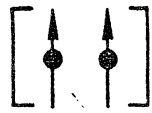



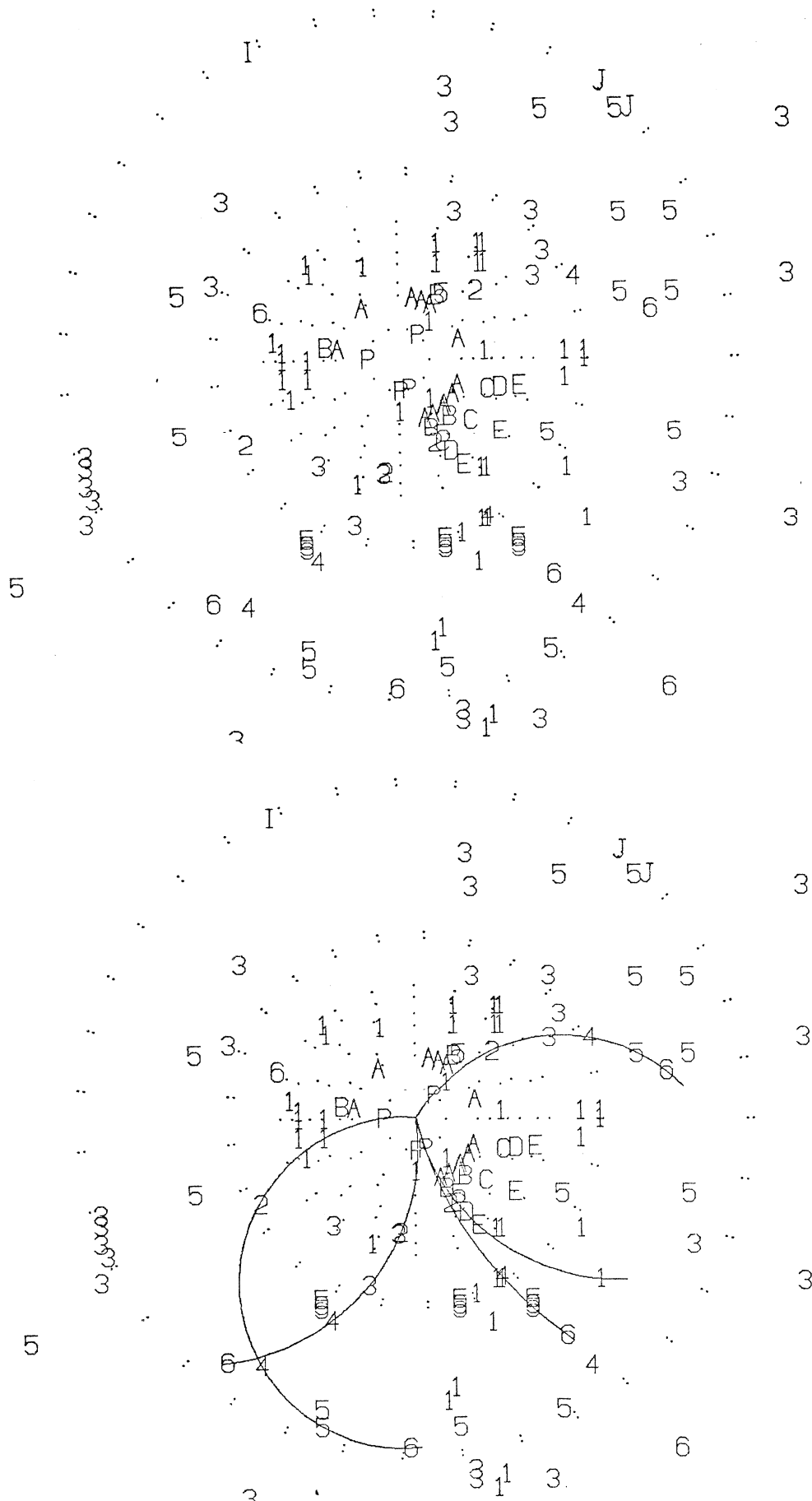
Fig. 3

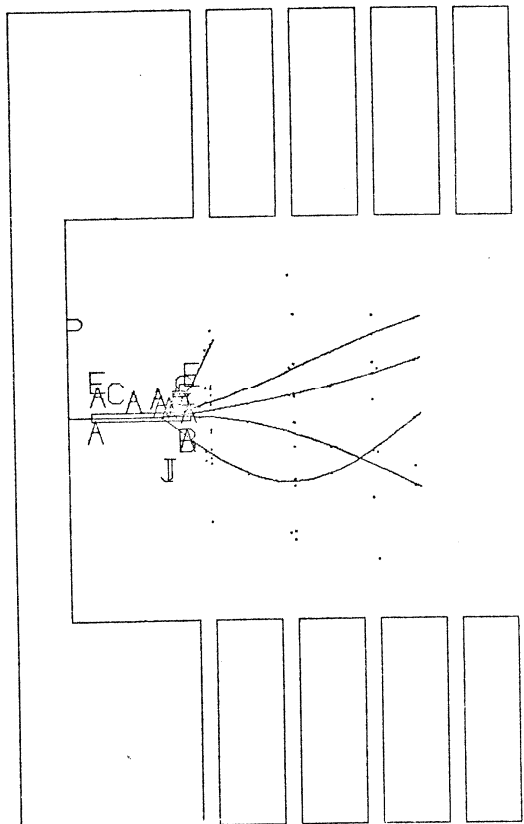
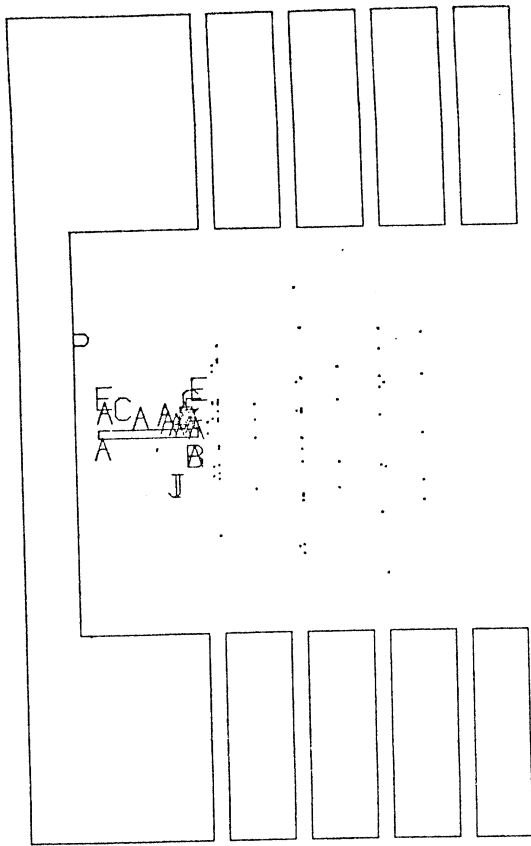
($s\bar{u}$ LEVEL SCHEME)

								
	S = 0				S = 1			
L	0	1	2	3	0	1	2	3
$C = (-1)^{L+S}$	+	-	+	-	-	+	-	+
	--- --- K'(1400)?? $\frac{Q_A}{1^{+-}}$ K(495) 0^{-+}	--- --- 1^{+-}	--- --- 2^{-+}	--- 3^{+-}	--- --- K*(1650)?? K*(890) 1^{--}	--- --- --- 2^{+} 1^{+} 0^{+}	--- --- 3^{-} 2^{-} 1^{-}	--- 4^{+} 3^{+} 2^{+} K*(1780)
							2^{+} 1^{+} 0^{+}	K*(1430) Q_B K(1400)??
	1S	1P	1D	1F	3S	3P	3D	3F

6-77
3215A7

Fig. 4





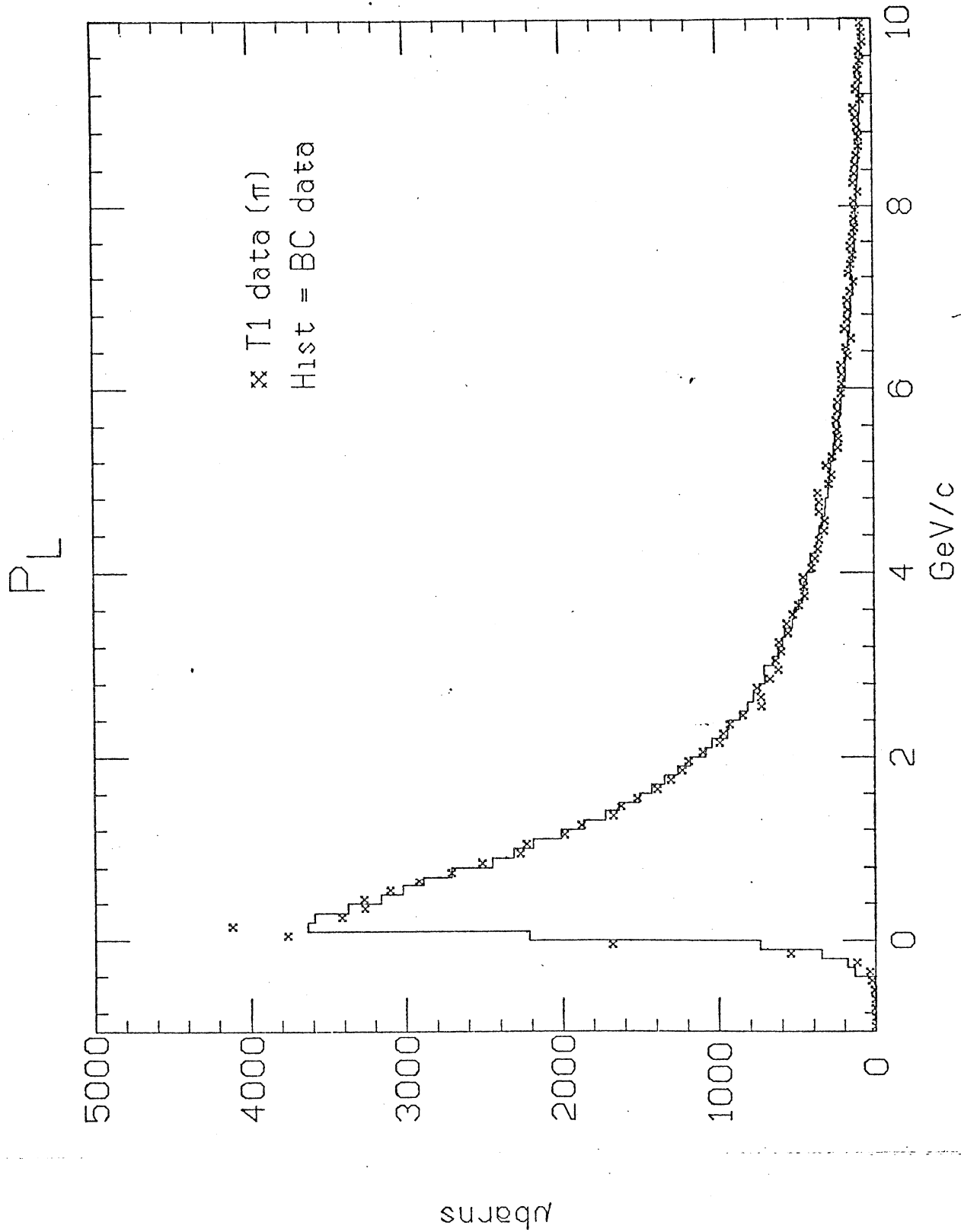


Fig. 7 (a)

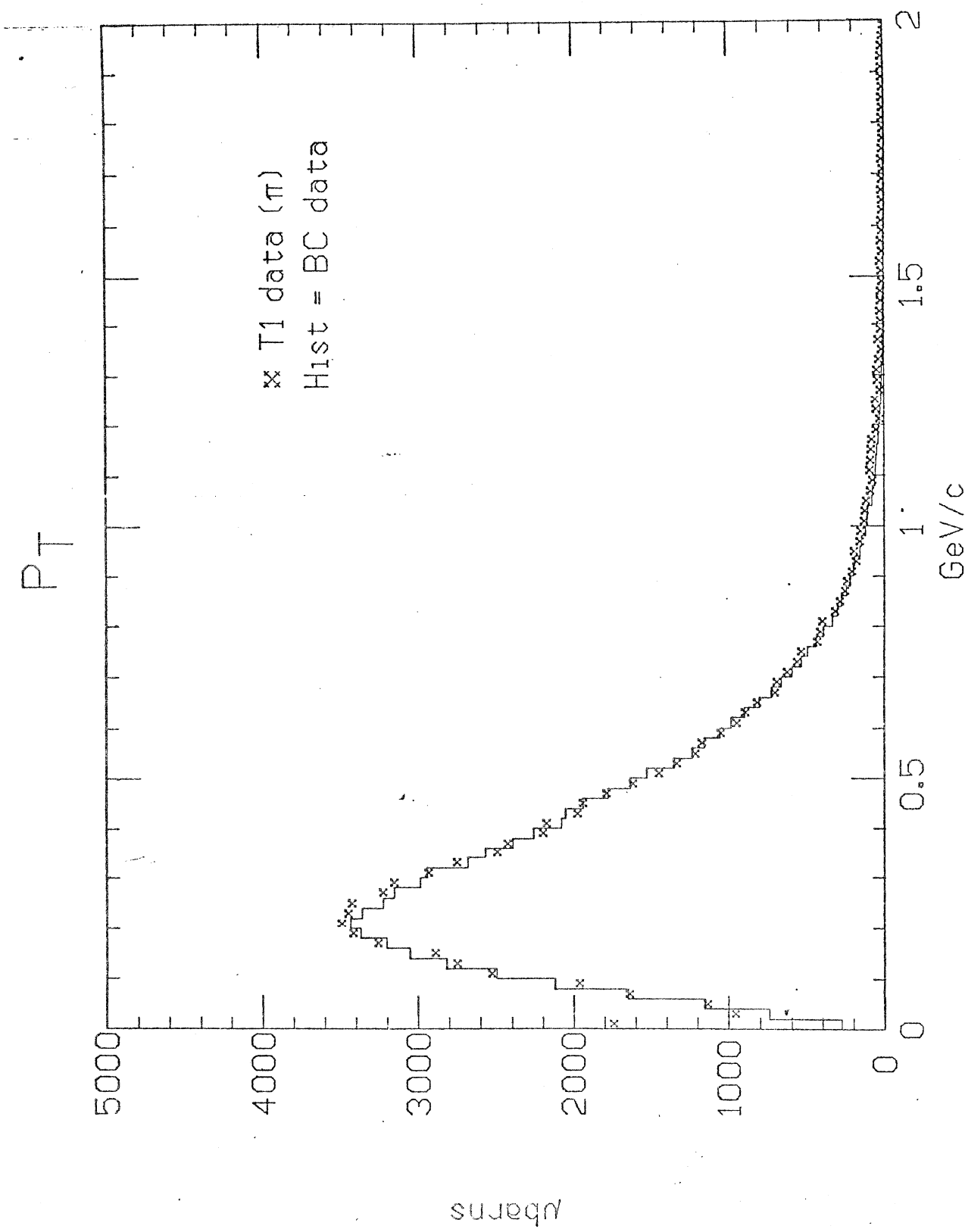


Fig. 7 (b)

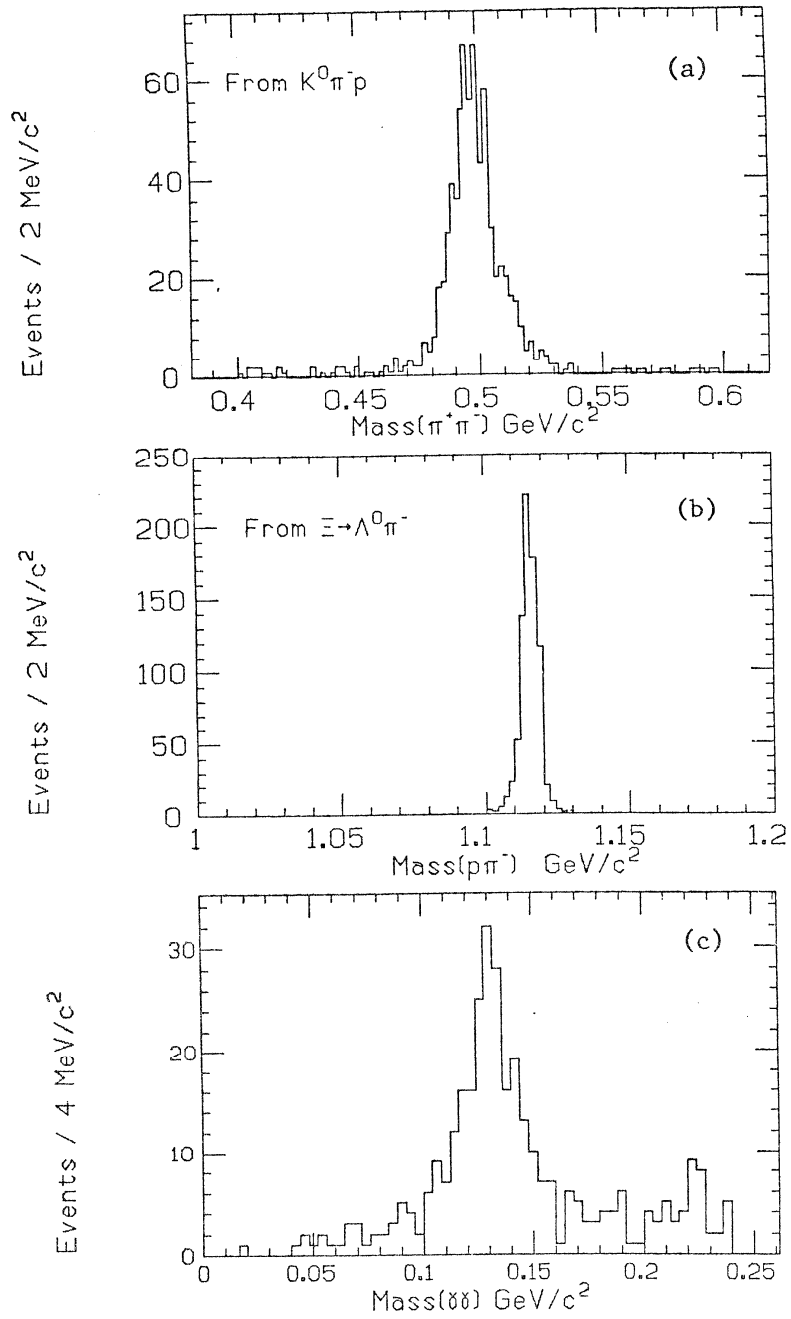


Fig. 8

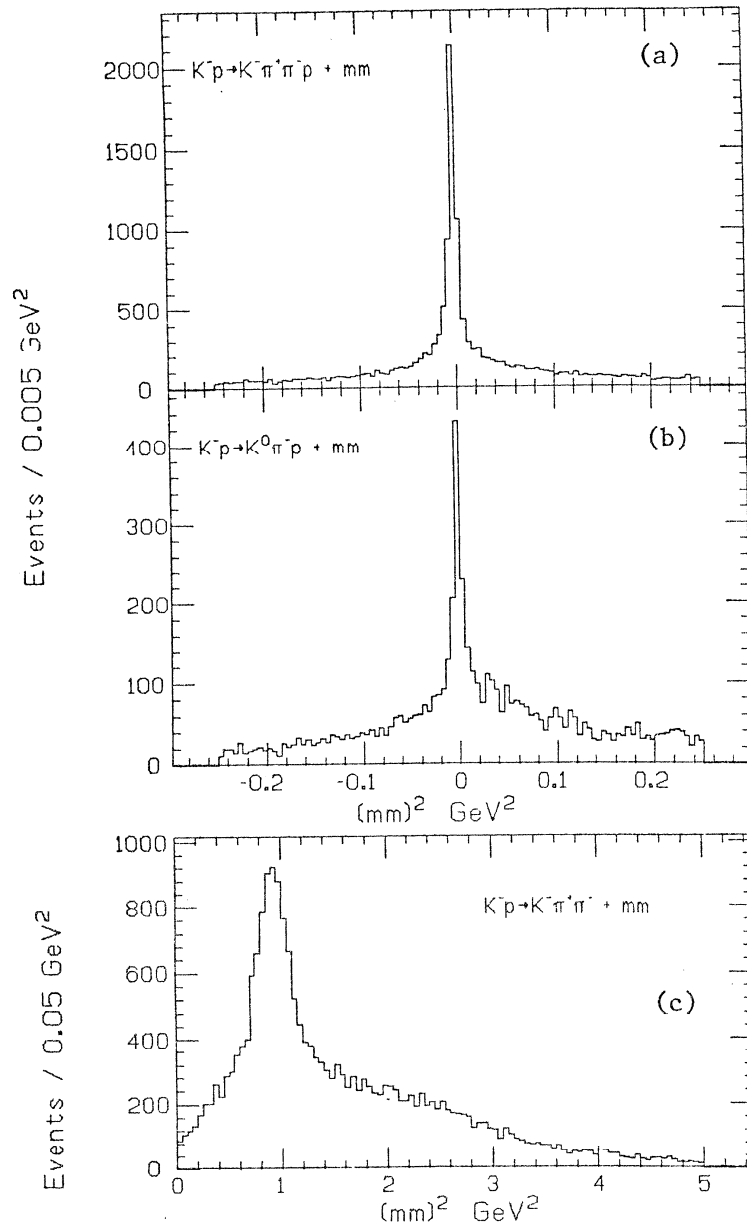
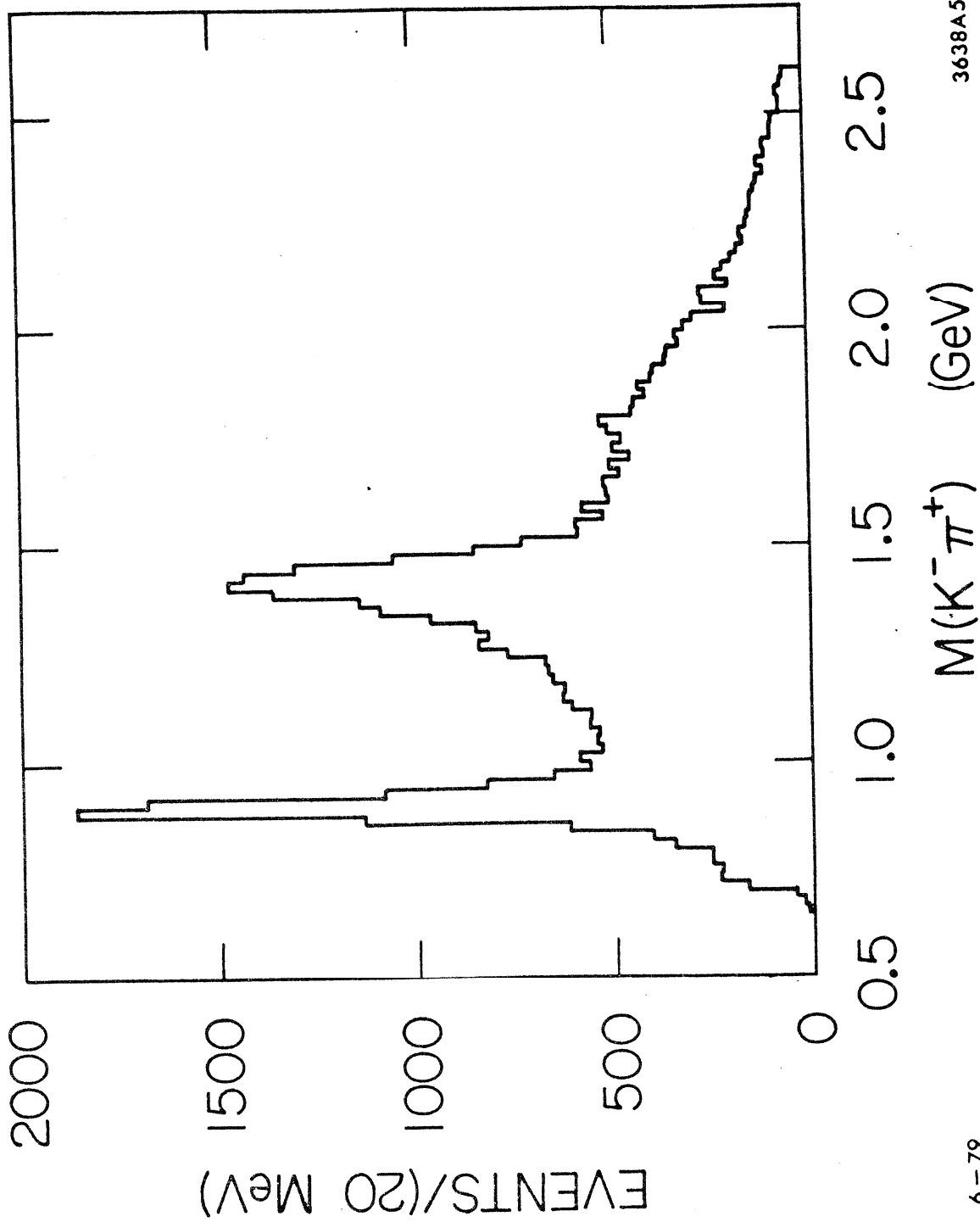


Fig. 9



3638A5

Fig. 10



FIG. 11

$M(K \pi \pi) \tau' < 1.0$ with $\Delta(1232)$ removed

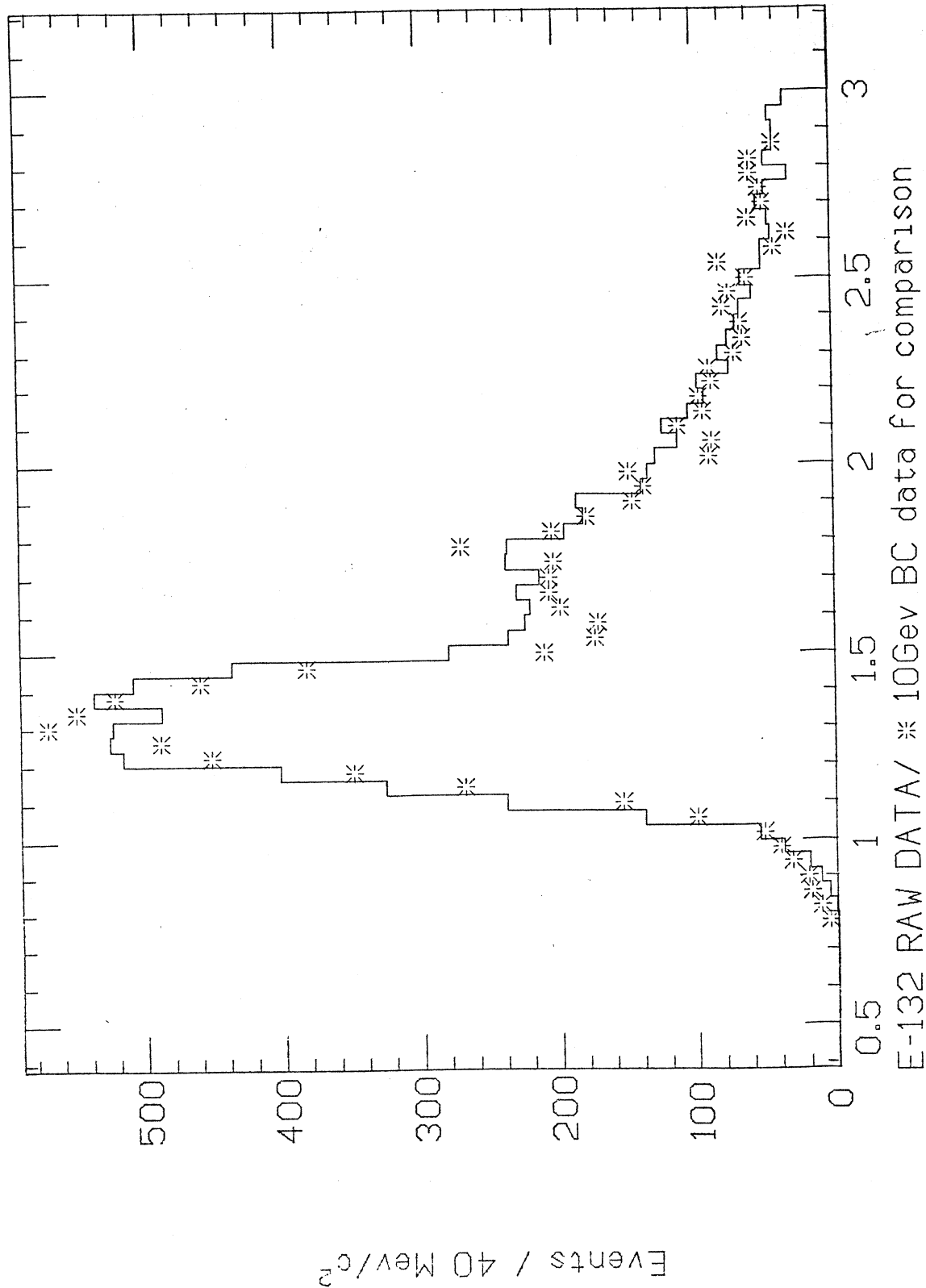


Fig. 12

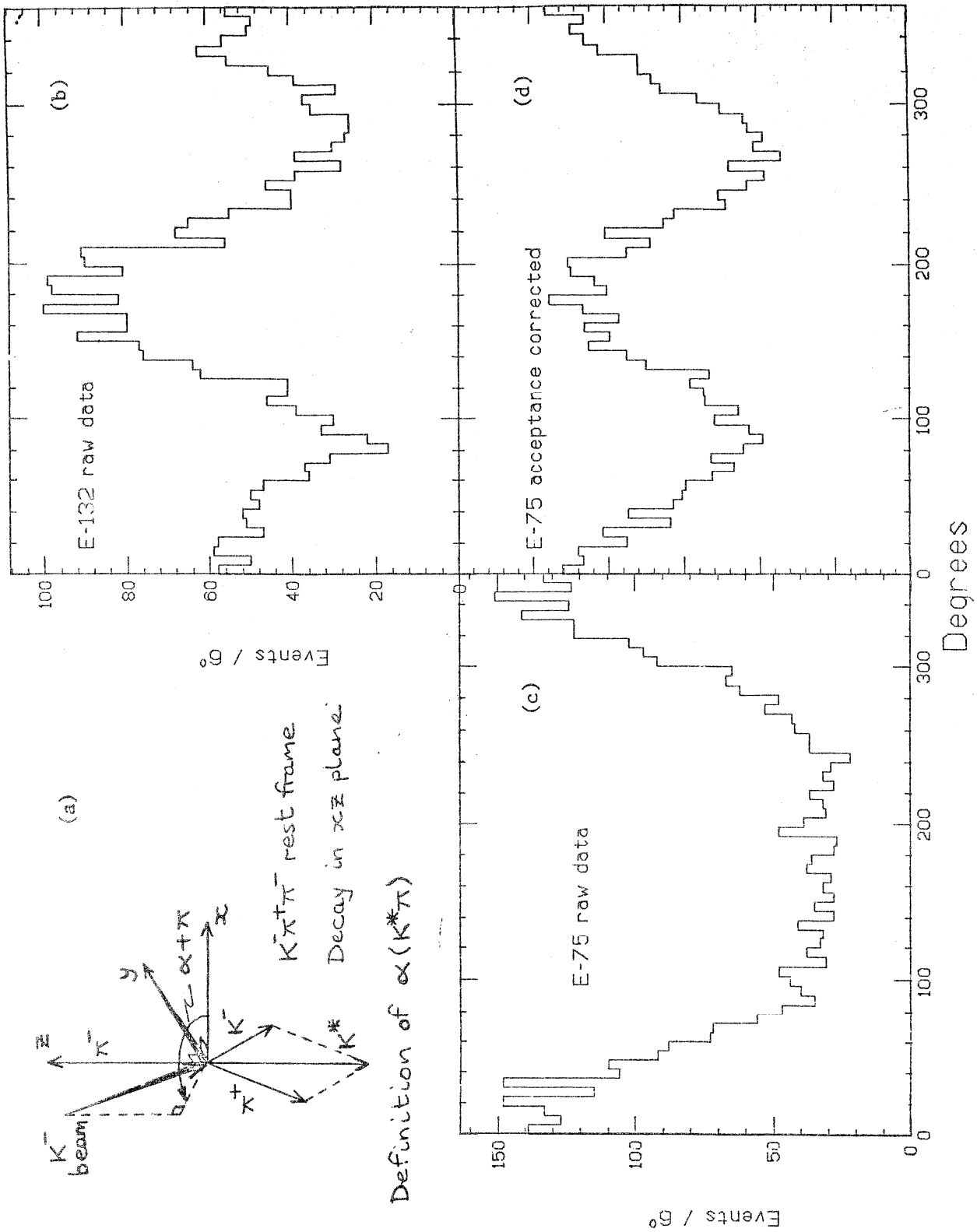


Fig. 13

K^0 C-of-M decay polar angle

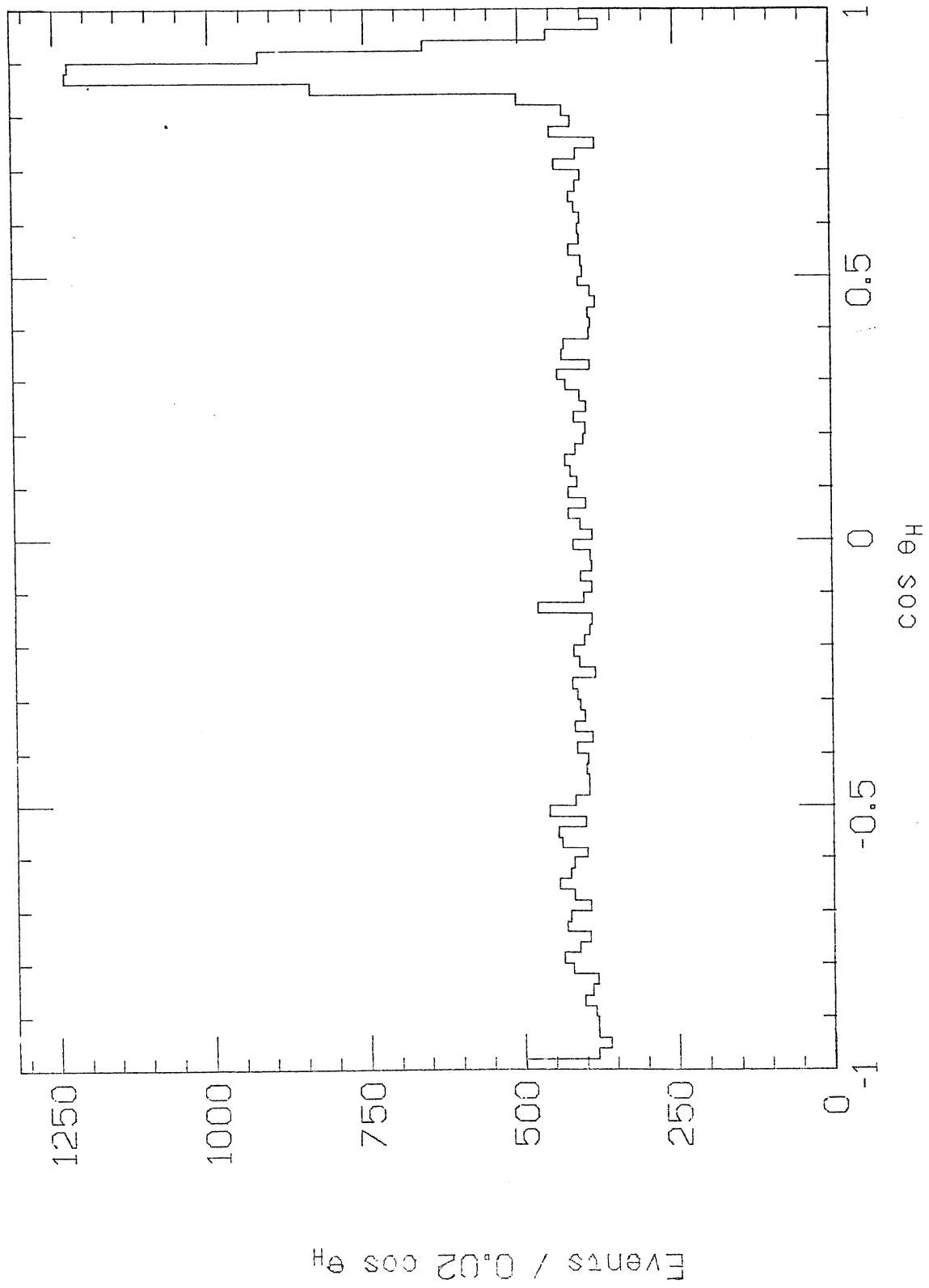


Fig. 14

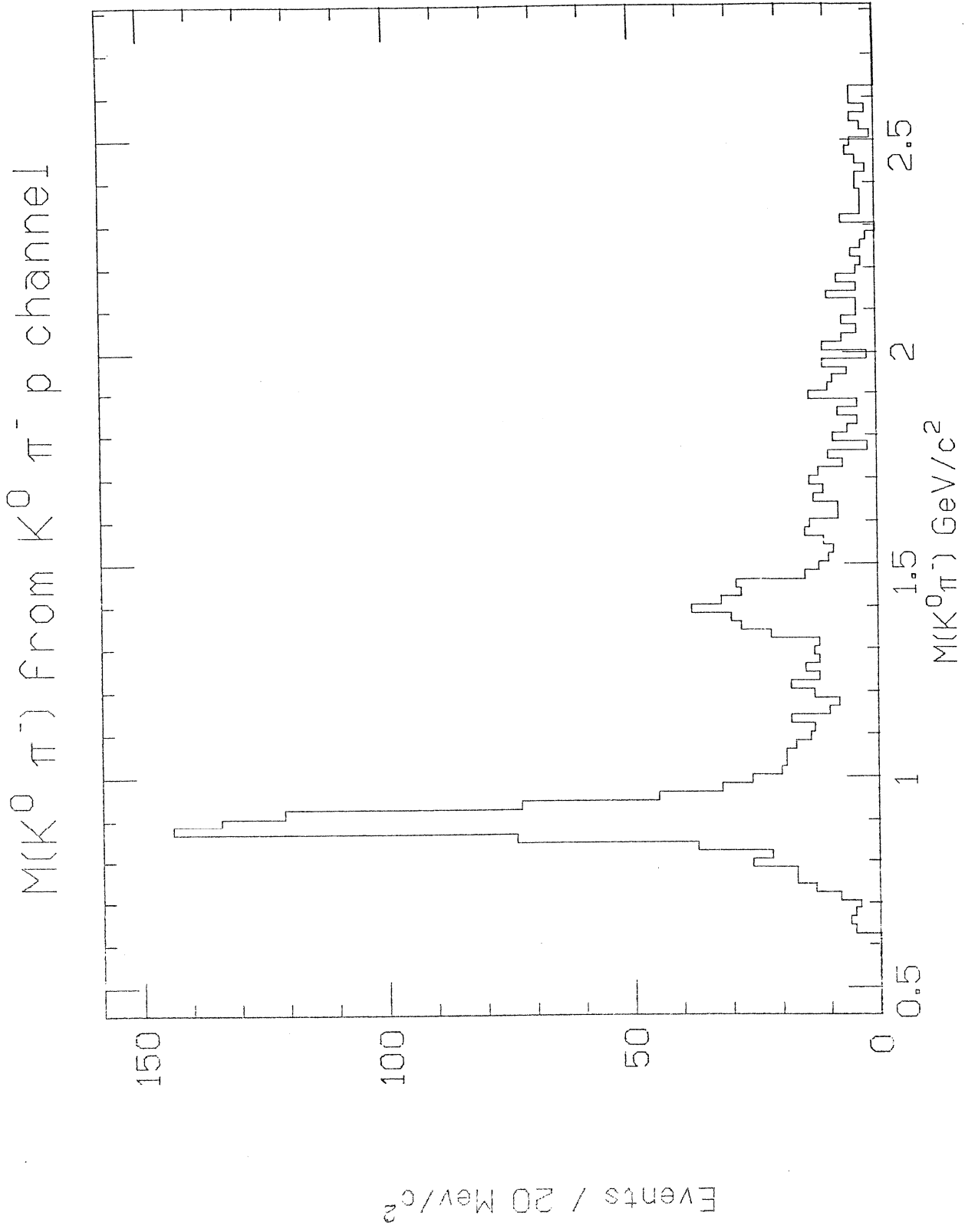


Fig. 15

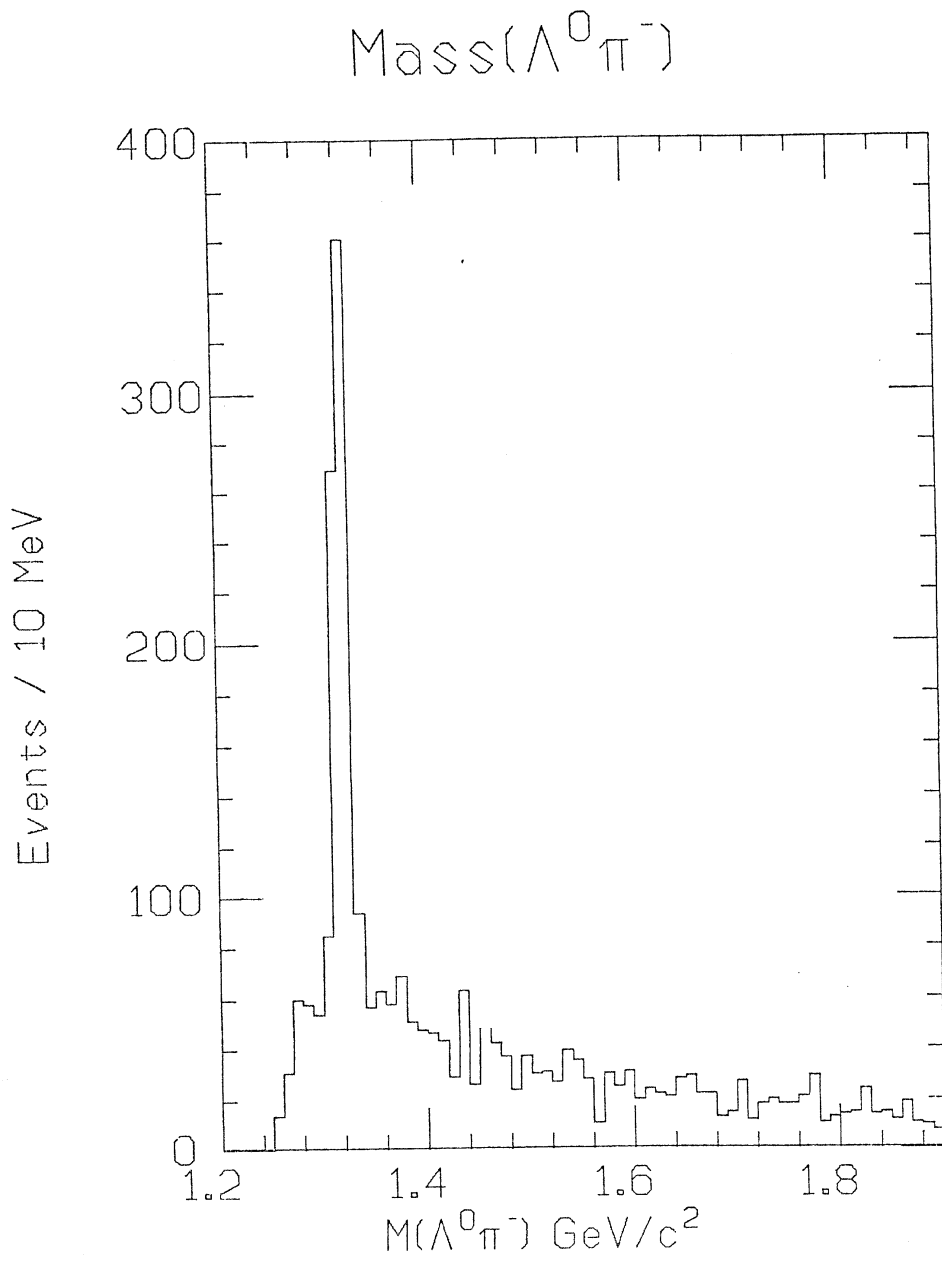


Fig. 16

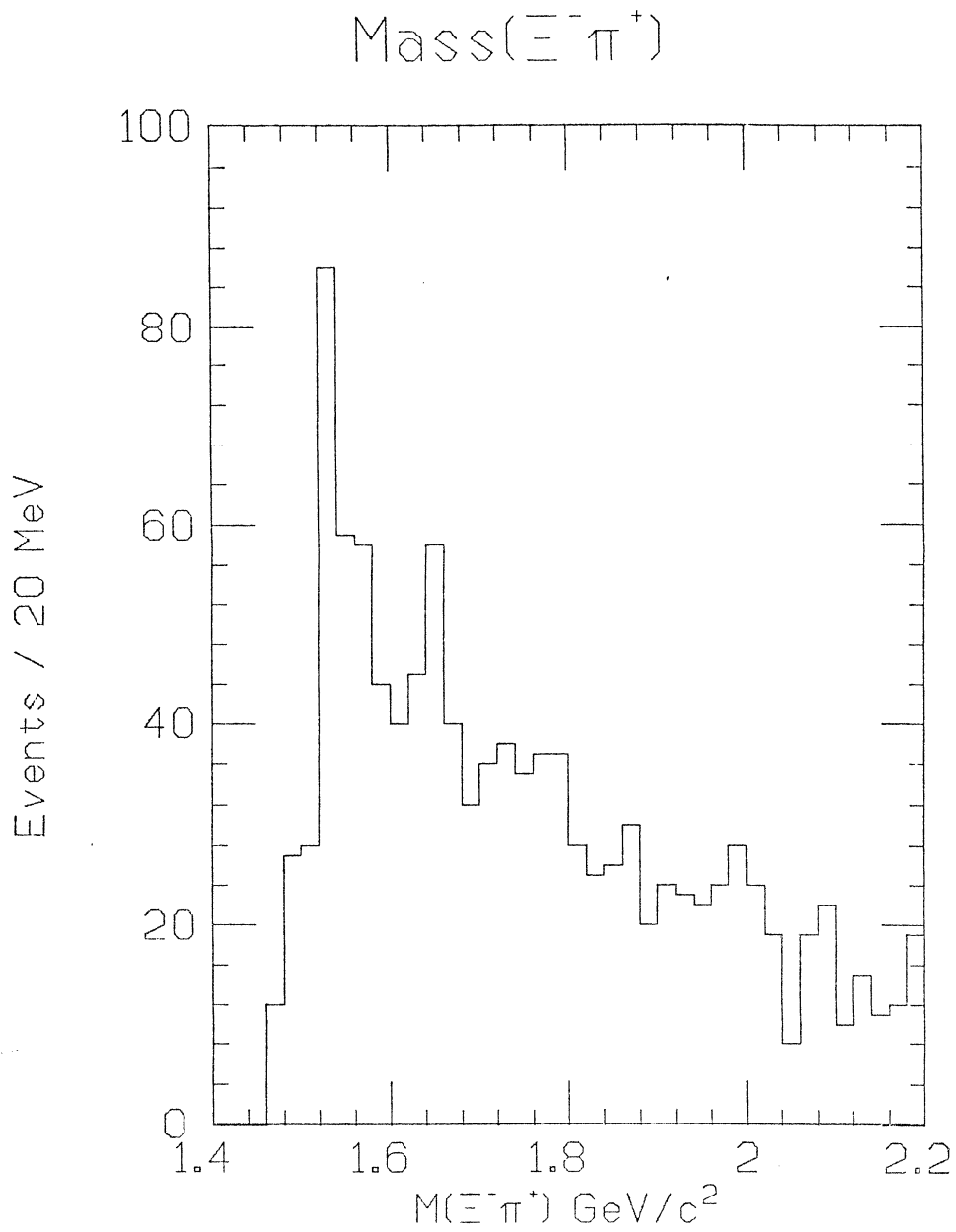


Fig. 17

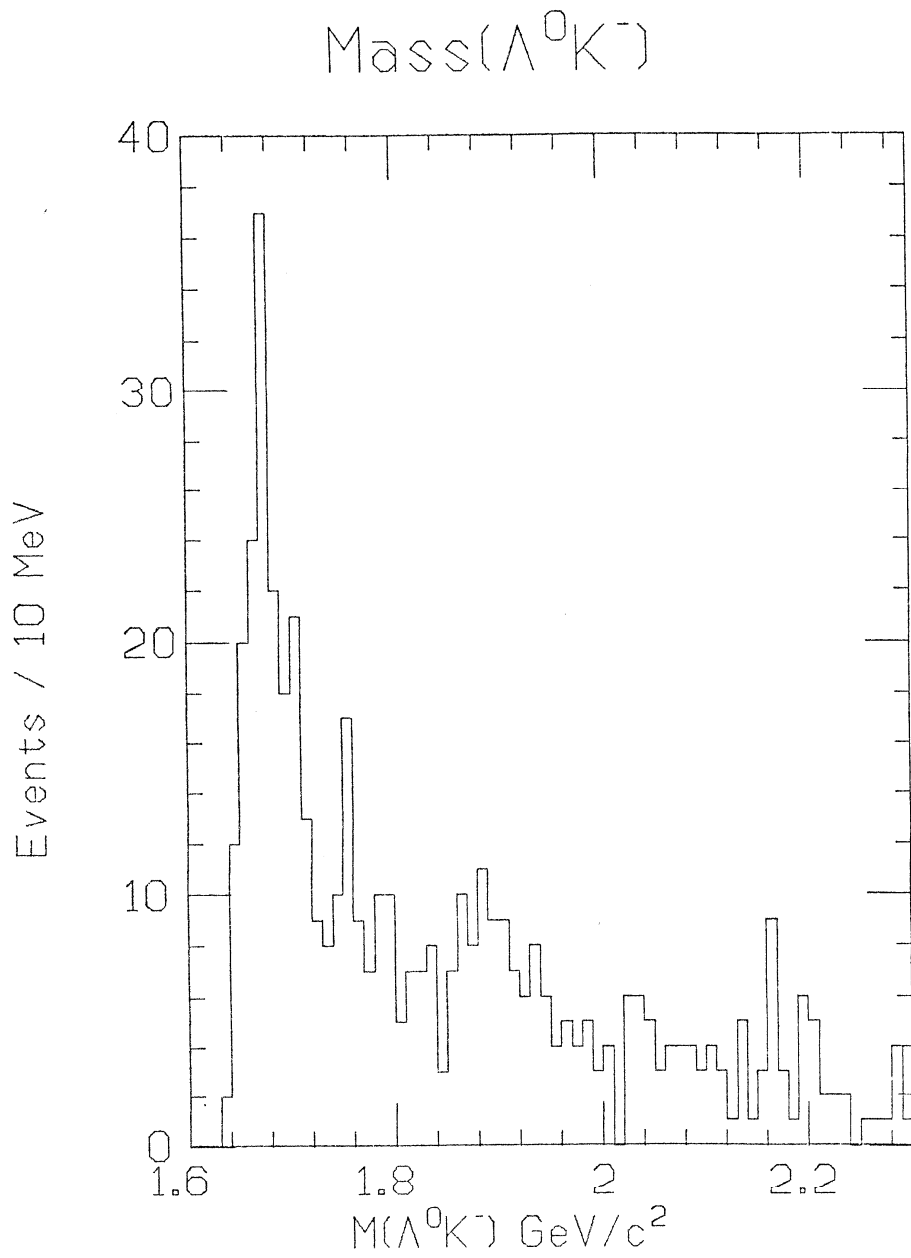
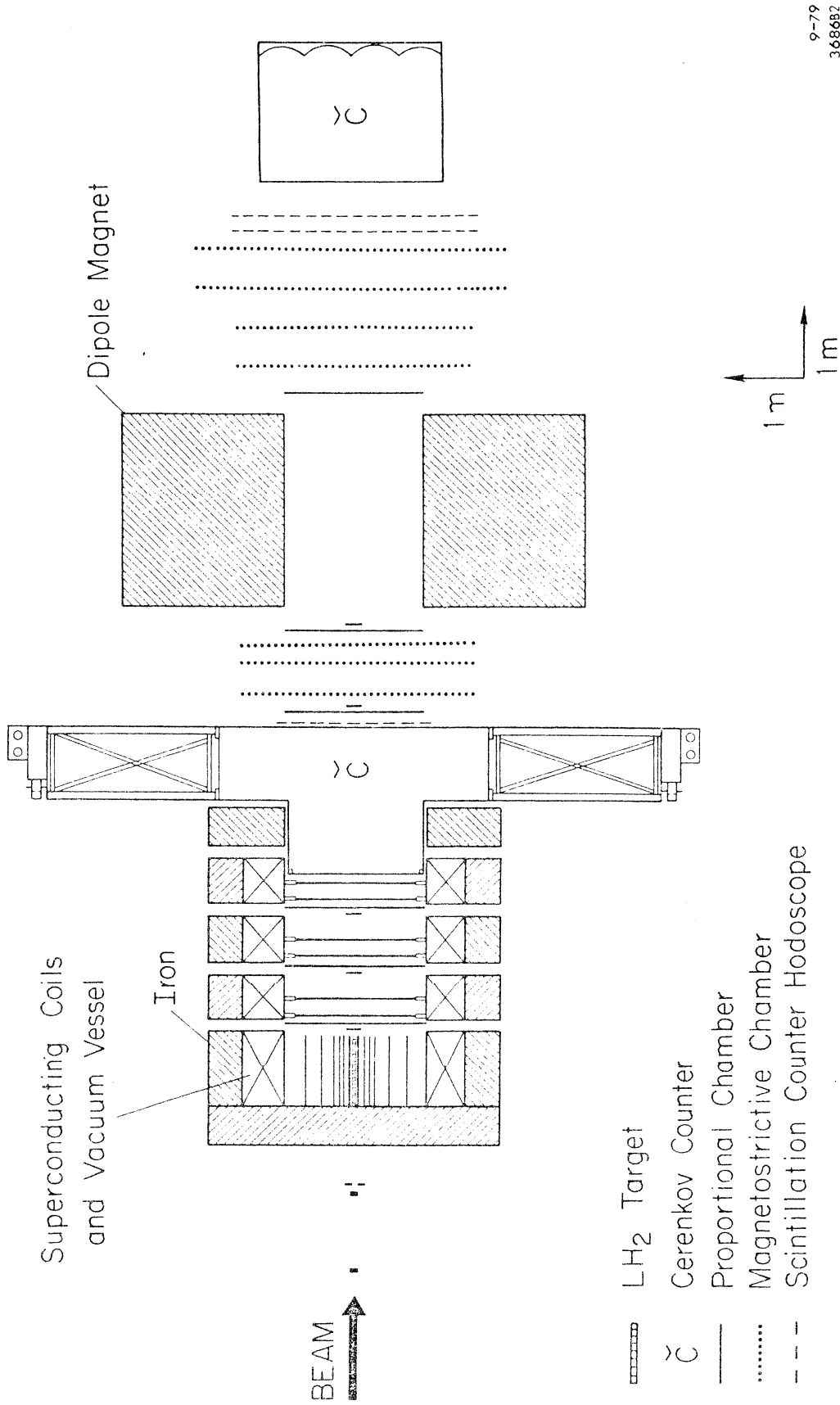


Fig. 18



- ▬ L₂H₂ Target
- Č Čerenkov Counter
- Proportional Chamber
- Magnetostrictive Chamber
- - - Scintillation Counter Hodoscope

Fig. 19

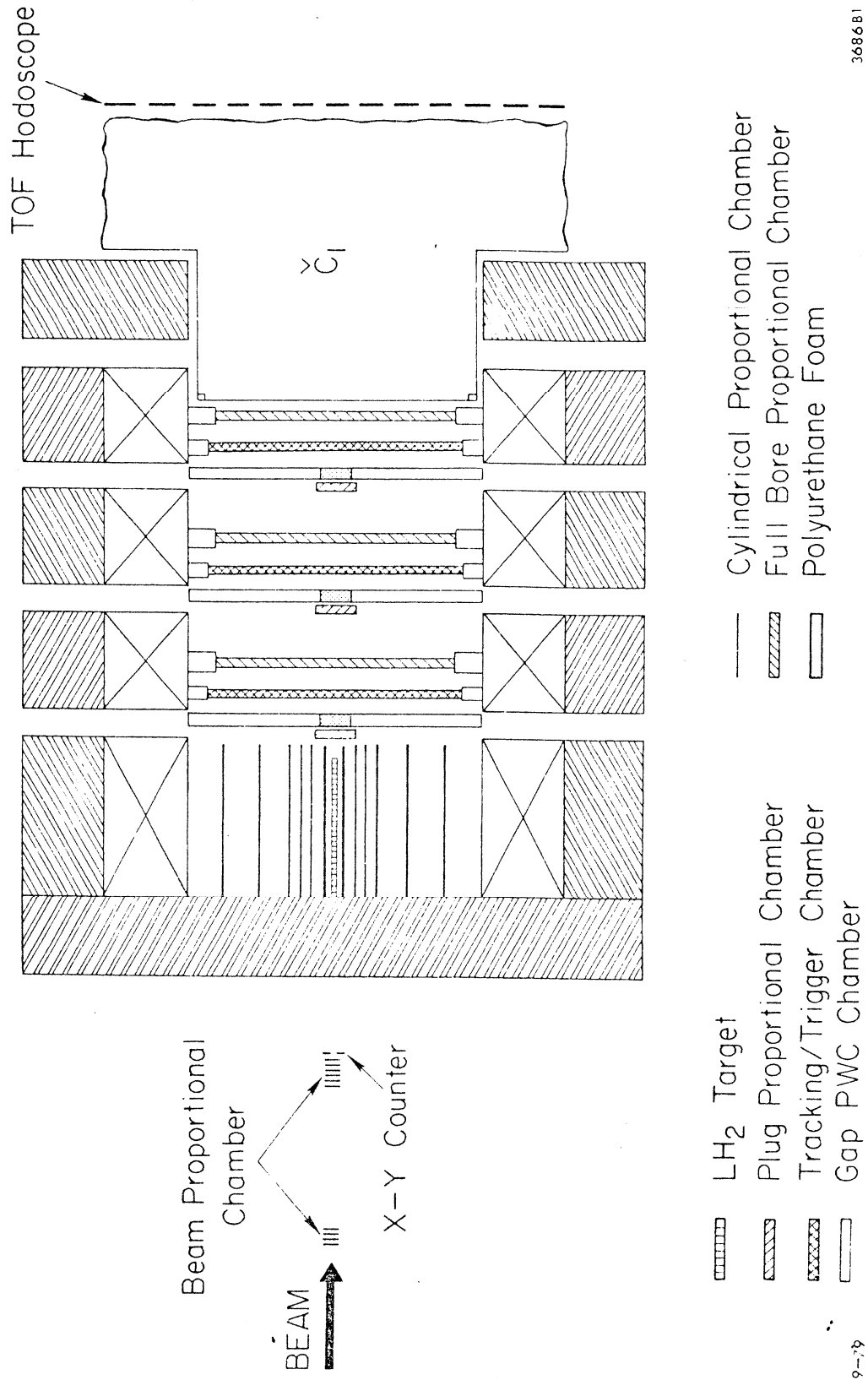


Fig. 20